SAND2016-0905R

EVALUATION OF THE FREQUENCIES FOR CANISTER INSPECTIONS FOR SCC

Fuel Cycle Research & Development

Prepared for
U.S. Department of Energy
Used Fuel Disposition Campaign

Christine T. Stockman (SNL)
***Charles R. Bryan (SNL)**

February 2, 2016
FCRD-UFD-2015-000510
SAND2016-0905R

*Corresponding author

UNCLASSIFIED UNLIMITTED RELEASE

Sandia National Laboratories is a multi-program laboratory managed and operated by Sandia Corporation, a wholly owned subsidiary of Lockheed Martin Corporation, for the U.S. Department of Energy's National Nuclear Security Administration under contract DE-AC04-94AL85000.

EXECUTIVE SUMMARY

This report fulfills the M3 milestone M3FT-15SN0802042, "Evaluate the Frequencies for Canister Inspections for SCC" under Work Package FT-15SN080204, "ST Field Demonstration Support – SNL". It reviews the current state of knowledge on the potential for stress corrosion cracking (SCC) of dry storage canisters and evaluates the implications of this state of knowledge on the establishment of an SCC inspection frequency. Models for the prediction of SCC by the Japanese Central Research Institute of Electric Power Industry (CRIEPI), the United States (U.S.) Electric Power Research Institute (EPRI), and Sandia National Laboratories (SNL) are summarized, and their limitations discussed. Some key points follow:

- Some of the most important processes and conditions thought to be involved in SCC at independent spent fuel storage installation (ISFSIs) have been described. Many of these factors are interdependent, so full parameterization for an empirical model would require a large data set. Currently, data are sparse and conflicting. Much was collected under conditions where at least one environmental condition (e.g., salt load) or material property (e.g., degree of sensitization) is set at a value that is at or beyond an extreme bound. Consequently crack initiation and growth rate data vary over several orders of magnitude.
- Considering this data, simplifying assumptions and professional judgment are used in current empirical models. Three empirical models for SCC at ISFSIs have been described and their limitations discussed. Their predictions of SCC growth rates penetration times vary greatly.
- It is the opinion of the authors of this report that currently available data and models do not provide a defensible technical basis for predicting a low probability of SCC penetration in 40 years. Thus, they have limited use in determining inspection frequency, and an operations-based and learning inspection frequency is necessary at this time.
- If it can be verified that the crack growth rate slows down by two orders of magnitude at a depth between 1 and 3 mm, or if a technically sound chloride density threshold model for relevant conditions can be established, prediction of low probability of SCC penetration in 40 years may be possible, especially for inland sites. Such predictions would provide the technical basis for site-specific inspection frequencies. The inspection required at license renewal can determine a chloride density distribution, which will provide input to and validation of the prediction of SCC at that particular site, thus, help determine the timing of a second inspection.
- A summary and evaluation of the sections of the Calvert Cliffs Dry Cask Storage AMP and NUREG-1927 R1 draft for comment (NRC 2015) relevant to SCC sample frequency have been provided.
- It is recommended that a comparison of the risk to the public from undetected through wall cracks and the dose to workers during inspections be performed to inform the inspection frequency and sample size.
- In the meantime (while additional data are collected and refined predictive models are developed), an operations-based and learning inspection frequency as indicated in Section 3.6.1.10 under "Learning AMPs (Aging Management Programs)" of NUREG-1927 R1 Draft for Comment (U.S. Nuclear Regulatory Commission (NRC) 2015) and recommended by the Nuclear Energy Institute (NEI) through their tollgates and learning AMPs (NEI 2014) is appropriate. Sample tollgates from Appendix A of NEI 13-03 (NEI 2014) are provided in Appendix B.

CONTENTS

EXECUTIVE SUMMARY iii

ACRONYMS ix

1. INTRODUCTION 1
   1.1 Recent Work 1
   1.2 The License Renewal Process and the Need for Establishing an Inspection Frequency 2
   1.3 Objective 3

2. PROCESSES AND CONDITIONS REQUIRED FOR SCC TO INITIATE AND PROPAGATE ON UNF CANISTERS 5
   2.1 Metal Susceptibility 5
   2.2 Tensile Stresses 5
      2.2.1 Residual Stresses from Welding 5
   2.3 Corrosive Environment on the Canister Surface 6
      2.3.1 Aqueous Conditions 6
      2.3.2 Corrosive Species 6
   2.4 Processes Involved in the Initiation and Propagation of SCC in Aqueous Solutions 6
      2.4.1 Crack Initiation 6
      2.4.2 Electrochemical Cell 7
      2.4.3 Cracking at the Tip 7
      2.4.4 SCC steps 9
      2.4.5 Parameters that May Influence the CGR in Aqueous Conditions 9
   2.5 Additional Processes Involved in the Possible Initiation and Propagation of SCC on UNF Canisters 10
      2.5.1 Deposit Composition 11
      2.5.2 Accumulation of Sufficient Chloride in the Canister Surface 13
      2.5.3 Areal Distribution of Deposits 15
      2.5.4 Deliquescence of Salts and the Limiting RH for Corrosion 16

3. PREDICTING SCC - AN OVERVIEW OF SOME RECENT SCC MODELS AND THE SIMPLIFYING ASSUMPTIONS MADE 19
   3.1 Model Overviews 19
      3.1.1 CREIPI 19
      3.1.2 EPRI 20
      3.1.3 SNL 24
      3.1.4 Summary 32
   3.2 Model Limitations 34
      3.2.1 CREIPI 34
      3.2.2 EPRI 36
      3.2.3 SNL 41
   3.3 Model Differences 42
   3.4 Conclusions on SCC Predictive Capability 43

4. FACTORS TO CONSIDER WHEN DETERMINING AN INSPECTION FREQUENCY 46

4.1 Site and Cask-Specific Crack Initiation Times and Growth Rate Predictions 46
4.2 Results of the Inspection of the Lead Casks 46
4.3 A Comparison of Risk 46

5. OVERVIEW OF THE ONLY EXISTING AMP AND NRC'S EXAMPLE AMP 48
5.1 Evaluation of Calvert Cliffs Dry Storage Canister Aging Management Program 48
5.2 Evaluation of NUREG-1927 Draft Revision 1 48

6. SUMMARY AND CONCLUSIONS 50

7. REFERENCES 52

APPENDIX A: Pertinent Sections of NUREG-1927 R1 Draft for Comment 58

APPENDIX B: NEI 14-03 Appendix A: SAMPLE TOLLGATES 66

FIGURES

Figure 2-1. Evaporation of seawater. a) Predicted brine composition as a function of concentration factor. b) Predicted salt phases as a function of concentration factor. 12

Figure 2-2. Predicted deliquescence behavior of salts that precipitate when seawater is evaporated (note that chemical formulas do not include waters of hydration). 17

Figure 3-1. DRH Models by EPRI (EPRI 2015c), Greenspan (1977), and sea salt data by He et al. (2014a). 23

Figure 3-2. Canister surface temperature map, for a decay heat load of ~7.6 kW (Suffield et al. 2012). 27

Figure 3-3. Crack growth rates as a function of K, calculated by the SNL probabilistic SCC model. 31

Figure 3-4. a) Measured crack growth rate data used to parameterize the CGR model in the SNL probabilistic model, b) Result of Monte Carlo estimation of uncertainty over Crack Growth Rate 32

Figure 3-5. Sample and crack geometry. 38

Figure 3-6. K_I as a function of location along the crack (bottom "tip" or surface), for different crack aspect ratios. 38

Figure 3-7. K_I as a function of aspect ratio, at the bottom of the crack, compared to inflection points in Shirai et al. (2011b) CGR data sets. 39

TABLES

Table 2-1. Measured Chloride Surface Density Thresholds Shown in Order of Increasing Chloride Densities in Solution. 14

Table 2-2. Measured Chloride Surface Density Thresholds at Relevant Conditions 14

Table 3-1. EPRI Sensitivity Cases 24

Table 3-2. Comparison of Models 33

Table 3-3. CRIEPI 4-Point Bend Test Results 35

Table 3-4. Possible surface drop dimensions for the CRIEPI 4-point bend tests 40

Table 3-5. Important SSC Model Differences and Limitations 43

ACRONYMS

ADAMS	the NRC Agency-wide Documents Access and Management System
AH	absolute humidity
AMP	Aging Management Plan/Program
AMR	ageing management review
ANL	Argonne National Laboratory
ASME	American Society of Mechanical Engineers
CCNPP	Calvert Cliffs Nuclear Power Plant
CSD	chloride surface density
CSDT	chloride surface density threshold
CFR	Code of Federal Regulations
CGR	crack growth rate
CISCC	chloride-induced stress corrosion cracking
CNWRA	Center for Nuclear Waste Regulatory Analysis
CoC	Certificate of Compliance
CRIEPI	Central Research Institute of Electric Power Industry, a research institute of the Japanese nuclear industry
DCSS	Dry Cask Storage System
DFC	draft for comment
DOE	U.S. Department of Energy
DOE NE	U.S. Department of Energy Office of Nuclear Energy
DRH	deliquescence relative humidity
DSC	Dry Storage Canister
Ea	activation energy
ENS	Enviro Nuclear Services
EPRI	Electric Power Research Institute
ERH	efflorescence re3lative humidity
ESCP	Extended Storage Collaboration Program
FMEA	failure modes and effects analysis
HAZ	heat affected zone
ISFSI	independent spent fuel storage installation
K_I	stress intensity factor

K_{ISCC}	threshold stress intensity factor for SCC
LANL	Los Alamos National Laboratory
NDA	United Kingdom Nuclear Decommissioning Authority
NDE	nondestructive examination
NEI	Nuclear Energy Institute
NOAA	National Oceanic and Atmospheric Administration
NRC	U.S. Nuclear Regulatory Commission
NUHOMS	Nutech horizontal modular storage
NUREG	publication prepared by staff of the U.S. Nuclear Regulatory Commission
NUREG/CR	technical report prepared by a contractor to the U.S. Nuclear Regulatory Commission
ORNL	Oak Ridge National Laboratory
PNNL	Pacific Northwest National Laboratory
PS	Proof Stress, usually defined as the stress that causes 2% strain
PWR	pressurized water reactor
RH	relative humidity
RH_L	limiting RH for corrosion
RIRP	regulatory issue resolution protocol
SAR	safety analysis report
SCC	stress corrosion cracking
SER	safety evaluation report
SNF	spent nuclear fuel
SNL	Sandia National Laboratories
SS	stainless steel
SSC	structure, system, and component
TLAA	Time-limited aging analysis
TWC	through-wall crack
UFDC	Used Fuel Disposition Campaign
UNF	used nuclear fuel
U.S.	United States

EVALUATION OF THE FREQUENCIES FOR CANISTER INSPECTIONS FOR SCC

1. INTRODUCTION

In the early years of dry storage of used nuclear fuel (UNF) in the United States (U.S.), licenses were granted for canister-based systems based on the assessment that the canisters would be in a warm, dry environment within the concrete casks or storage modules, and that no corrosion of the stainless steel (SS) canisters (304 SS, 304L SS, 316 SS or 316L SS) would occur within the 20-year license period. As some initial site license periods have expired and license renewals are taking place, the conclusion that no corrosion will take place during the license renewal period has been re-examined, and the possibility of atmospheric chloride induced stress corrosion cracking (CISCC) compromising the confinement safety function is being researched. The work by the U.S. nuclear industry, the U.S. Nuclear Regulatory Commission (NRC), the U.S. Department of Energy (DOE) laboratories, and the international community has been shared and partially coordinated by a volunteer committee - the Extended Storage Collaboration Program (ESCP), chartered in 2009 by the U.S. Electric Power Research Institute (EPRI).

1.1 Recent Work

In early 2011, the Nuclear Energy Institute (NEI) and the NRC initiated the regulatory issue resolution protocol (RIRP) for issue number RIRP-N-10-01 "Dry Spent Fuel Storage Canister Stress Corrosion Cracking in Coastal Marine Atmospheres". As stated in a recent screening plan (NRC 2014a):

> *"Industry and NRC will interact in public meetings and through letters to achieve the following: Consistent with the data acquired, the following are determined and documented: 1. The conditions of canister materials and environment under which CISCC could potentially initiate. 2. The time scales under which CISCC could occur, based upon actual atmospheric and cask conditions. 3. Agreed upon Susceptibility Assessment Criteria that can be used by licensees to evaluate the potential for CISCC to occur on canisters at their site."*

In response to these meetings, EPRI has committed to producing several reports. Already completed reports are:

1. R&D Roadmaps (EPRI 2013a and EPRI 2014a),
2. A Failure Modes and Effects Analysis (FMEA) (EPRI 2013b),
3. A literature review (EPRI 2014b), and
4. A Flaw Growth and Tolerance Report (EPRI 2014c).
5. A susceptibility criteria report (EPRI 2015)

In producing these reports, EPRI has been developing and continually improving a deterministic stress corrosion cracking (SCC) growth rate model. It plans to convert this model into a probabilistic one for a "Canister Confinement Integrity Assessment" report (due the beginning of 2016) that will analyze the benefit of various monitoring, mitigation, & inspection regimes and develop a report providing "Aging Management Guidelines" by the end of 2016 (Broussard and Chu 2015). In addition there is an ongoing project to develop nondestructive evaluation (NDE) techniques for inspecting canisters (Renshaw 2014).

At the same time, the NRC has conducted significant work including:

1. Production of a data gap analysis and research prioritization report which concludes that two areas should be addresses first, one of which is "Stress corrosion cracking (SCC), pitting, and crevice corrosion of stainless steel canister body and welds" (NRC 2014b),
2. Sponsorship of research on the conditions necessary for atmospheric CISCC including seminal reports by Caseres and Mintz (2010) and He et al. (2014a), and methods for monitoring those conditions and inspecting canisters for CISCC including reports by He et al. (2014b) and Meyer et al. (2013).
3. Approval of a license renewal for the Calvert Cliffs independent spent fuel storage installation (ISFSI) which includes an Aging Management Plan/Program (AMP) for the Dry Storage Canister (DSC) external surfaces (NRC 2014c), and
4. Development of a draft revision of NUREG-1927, which includes an "Example AMP for Localized Corrosion and Stress Corrosion Cracking of Welded Stainless Steel Dry Storage Canisters" (NRC 2015).

The DOE Laboratories have provided input into these activities and have conducted research and analyses as summarized by Stockman et al. (2014), including[a]:

1) Fourteen reports on the conditions necessary for atmospheric chloride induced crevice corrosion and SCC and the rate of initiation and propagation of these processes (mainly by researchers at Sandia National Laboratories (SNL) between 3/30/11 and 7/24/15),
2) Nine thermal calculations as input to the thermochemical environment on the canisters (mainly by researchers at the Pacific Northwest National Laboratory (PNNL) between 03/31/11 and 9/30/14),
3) Eight reports evaluating or developing techniques for inspecting canisters for CISCC (mainly by researchers at PNNL and Los Alamos National Laboratory (LANL) between 08/30/12 and 09/18/14), and
4) Four reports developing AMPs for CISCC (mainly by researchers at Argonne National Laboratory (ANL) between 06/30/12 and 09/26/14).

1.2 The License Renewal Process and the Need for Establishing an Inspection Frequency

10 CFR 72.42(a) states:

> *"… Application for ISFSI license renewals must include the following: (1) TLAAs that demonstrate that structures, systems, and components important to safety will continue to perform their intended function for the requested period of extended operation; and (2) A description of the AMP for management of issues associated with aging that could adversely affect structures, systems, and components important to safety."*

NUREG-1927 (NRC 2011) provides further guidance on how to achieve this, suggesting the applicant perform an ageing management review (AMR) and identify all structures, systems, and components (SSCs) that are important to safety (ITS), and identify all aging mechanisms that might impact the ability

[a] Many of the DOE reports have not yet been released to the public, including the report by Stockman et al. (2014). However, the Stockman et al. (2014) report should be made publically available soon, and it provides links to the DOE reports through 2014 that are publically available.

of these SSCs to perform their safety functions within the license period. In dry cask storage systems (DCSSs) with SS canisters performing the confinement function, those canisters are ITS SCCs and CISCC has been identified as an aging mechanism that could impact their confinement function (NRC 2012). As stated by the regulation above, once an ageing mechanism is identified, the applicant must perform a TLAA that demonstrates the ITS SCC continues its safety function or describe an AMP to monitor and control the degradation of the SSC. At this time, the uncertainty in the predictive models of CISCC of SS canisters is too large for applicants to successfully use the TLAA approach. Therefore, until further research and/or operating experience is obtained to reduce this uncertainty, the AMP approach is needed. NUREG-1927 is currently being updated with more detail concerning AMPs and a draft for comment (DFC) has been issued (NRC 2015). This update provides more detail on the 10 elements of an effective AMP. The fourth element "Detection of Aging Effects" is described in Section 3.6.1.4:

> *"Detection of aging effects should occur before there is a loss of intended function for any SSC identified within the scope of the program. This element should include inspection and monitoring details, including method or technique (i.e., visual, volumetric, surface inspection), frequency, sample size, data collection, and timing of inspections to ensure timely detection of aging effects."* Thus, the applicant needs to establish an **inspection frequency** in its license application or supporting documents.

In order to establish and justify the timing of initial inspections and the frequency of inspections thereafter, it is necessary to be able to predict the timing of SCC initiation and the crack growth rate (CGR). At this time, the uncertainty in these predictions is large, however, in its description of AMPs, the NRC acknowledges that information may be incomplete at the time of license application and there may be a need for adjustments to the AMP as new information is obtained. As stated in Section 3.6 of NUREG-1927 R1 DFC (NRC 2015):

> *"An effective AMP prevents, mitigates, or detects the aging effects and provides for the prediction of the extent of the effects of aging and timely corrective actions before there is a loss of intended function. Aging management programs should be informed, and enhanced when necessary, based on the ongoing review of both site-specific and industry-wide operating experience, including relevant international and non-nuclear operating experience. Operating experience provides direct confirmation of the effectiveness of an AMP and critical feedback for the need for improvement. As new knowledge and data become available from new analyses, experiments, and operating experience, licensees and Certificate of Compliance (CoC) holders should revise existing AMPs (or pertinent procedures for AMP implementation) to address program improvements or aging issues."*

1.3 Objective

This report provides an evaluation of the current state of knowledge pertinent to establishing an SCC inspection frequency and identifies the issues contributing to the uncertainty in determining this frequency.

2. PROCESSES AND CONDITIONS REQUIRED FOR SCC TO INITIATE AND PROPAGATE ON UNF CANISTERS

In order for SCC to occur, three criteria must be met: the metal must be susceptible to SCC, sufficient tensile stress must be present to support SCC, and a corrosive environment must exist. Once these conditions are met, a series of processes must occur for SCC to initiate and propagate. These have been well described in the literature, but a brief listing and discussion of the processes and conditions that effect SCC initiation and propagation rates are listed and briefly discussed here as a background for the discussions in Section 3.

2.1 Metal Susceptibility

The canister metals are austenitic SSs, including 304/304L SS and 316/316L SS, which are known to be susceptible to SCC. However, the degree of susceptibility is a function of several factors, including the degree of sensitization, the degree of cold working, the presence of iron contamination on the metal surface, and the surface finish (Parrott and Pitts, 2011).

Sensitization occurs when the metal is heated during welding. In the heat-affected zone (HAZ), Cr diffuses from the metal grains into the grain boundaries, where it combines with carbon to form chromium-rich carbides. This results in chromium-depleted zones at grain boundaries that are more susceptible to localized corrosion. Hence, sensitized materials are subject to grain boundary attack. Material vulnerability to sensitization is a function of metal composition, with 304 SS being more vulnerable than 316 SS, and the carbon-poor varieties 304L SS and 316L SS being least vulnerable. However, full sensitization (formation of chromium depleted zones at all grain boundaries) is not required to affect corrosion susceptibility; even small degrees of sensitization can be important.

Cold work can adversely affect the corrosion resistance of SSs (e.g., Khatak et al. 1996; Parrott and Pitts 2011). First, it results in the formation of extensive dislocation structures within the metal matrix, which can result in the formation of regions where destabilization of the protective oxide layer is more likely and the ability of the material to repassivate is degraded (Peguet et al. 2007), increasing the susceptibility to localized attack. For large deformation, the formation of strain-induced martensite in the metal is possible, which is less resistant to corrosion than austenite. SCC crack growth rates have also been observed to increase with increasing cold work, particularly at 20% cold work and above (Kuniya et al. 1988). In general, for interim storage canisters, the degree of cold work will be small, as that associated with plate manufacture will be annealed out prior to plate delivery. Bending the plates into a cylinder is anticipated to impart only a few percent cold working to the metal. However, on a local scale, grinding and cutting processes, and accidental impacts during cask manufacturing, can impart high degrees of cold work, and areas affected by this may serve as loci for enhanced corrosion.

A rough surface finish (>1 μm) can promote initiation of corrosion, apparently by trapping water and chloride ions on the surface (Parrott and Pitts 2011). Also, surface grinding can produce large local variations in stress that may contribute by increasing strain energy and the dissolution rate of the metal. All storage canisters have rougher surfaces than 1 μm.

2.2 Tensile Stresses

2.2.1 Residual Stresses from Welding

The only large tensile stresses expected on UNF canisters are the residual stresses formed during welding in the weld and HAZ. Direct measurements of the stresses present in typical canister weld regions are in progress, but results are not yet available. However modeling by the NRC (Kusnick et al. 2013) predicts

through-wall tensile stress greater than or equal to the yield strength of the metal parallel to the weld. Such stresses could support through-wall stress corrosion cracks perpendicular to the weld within the HAZ.

2.3 Corrosive Environment on the Canister Surface

For SCC to occur, aqueous conditions must be present on the canister surface, and a corrosive species (chloride, for CISCC) must also be present.

2.3.1 Aqueous Conditions

The concrete overpack or storage module protects the canister from direct rain and snowfall, but with intense winds, some precipitation may enter the cooling vents in these structures and contact the canister. Any such contact however, is expected to be brief because the canister is warmer than the ambient environment and evaporation will occur. However, there is another avenue for aqueous conditions to form on the canister. For most dry cask storage systems, passive ventilation is utilized to cool the canisters within the overpacks, and large volumes of outside air are drawn through the system. Dust and aerosols within the air are deposited on the canisters, and as the canisters cool over time, salts in the dust will deliquesce to form brine on the storage container surface.

2.3.2 Corrosive Species

The dusts and aerosols deposited on the canister may include corrosive species. Of special interest to SCC of 304 SS is chloride. Significant chloride deposition is most likely to occur at locations were airborne chloride is present, such as near salt water bodies (e.g. the ocean), adjacent to cooling towers, or in close proximity to roads that are periodically treated with deicing salts.

2.4 Processes Involved in the Initiation and Propagation of SCC in Aqueous Solutions

An overview of SCC crack initiation and propagation mechanisms and models for metals in aqueous solutions is provided by Jones (2003). Many mechanisms and models have been proposed, but they all include an electrochemical cell that drives a dissolution process and most include a mechanical mechanism for cracking of the metal at the crack tip under tensile stress. These two work together in synergistic fashion to result in crack formation and propagation that could not occur with just one alone. The overview by Jones (2003) and an example of electrochemical corrosion are is briefly described below.

2.4.1 Crack Initiation

Jones (2003) discusses crack initiation by three processes:

- Crack Initiation at Surface Discontinuities
- Crack Initiation at Corrosion Pits
- Crack Initiation by Intergranular Corrosion or Slip Dissolution

However, he states

> *"Although the features causing SCC initiation, such as pits, fabrication defects, and intergranular corrosion, are observed and identified easily, there are few well-developed models of SCC initiation."*

Since 2003, there has been considerable experimental work and model development for pit growth and SCC initiation from pits under atmospheric conditions, some of which is reflected in the SCC model developed by SNL (Section 3.1.3.3).

2.4.2 Electrochemical Cell

A good example of an electrochemical cell driving localized corrosion of a passive metal is provided by pit corrosion of a SS in a NaCl solution. Electrochemical corrosion can be divided into three parts, anodic processes, cathodic processes, and transport of ions between the anode and cathode within the brine layer. For a pit, the anodic processes occur at the anode which is at the base of the pit where oxidative dissolution of metal occurs (for example $M \rightarrow M^{x+}(aq) + x\ e^-$) and electrons enter the conducting metal. Hydrolysis of the metal cation to form a metal hydroxide or oxy-hydroxide releases H^+, thus acidifying the brine within the pit. An example of an intermediate step is ($M^{+2} + H_2O \rightarrow MOH^+ + H^+$). An example of an overall reaction is ($M^{3+} + 2\ H_2O \rightarrow MO(OH) + 3H^+$). The cathodic processes consume electrons by reduction of oxygen to form the hydroxide ion ($O_2 + 2\ H_2O + 4e^- \rightarrow 4\ OH^-$) and/or reduction of the hydrogen ion to form a hydrogen radical or hydrogen molecule ($H^+ + e^- \rightarrow H\bullet$) or ($2H^+ + 2\ e^- \rightarrow H_2$). At the metal surface where O_2 from the air is available, reduction of oxygen occurs and the pH rises. The reduction of the hydrogen ion only occurs at a significant rate in acid solutions and this reaction also acts to raise the pH. For now only the reduction of oxygen is considered.

Electrons produced at the pit bottom (the anode) flow through the conducting metal to the surface (the cathode) where they are consumed. The electrical circuit is completed by migration of ions between the cathode and the anode. In this system, ion migration will likely be dominated by chloride anions migrating from the cathode to the bottom of the pit and the migration of sodium and metal cations out of the pit. Thus the brine on the surface becomes enriched in NaOH, and the brine at the pit bottom becomes enriched in HCl that can dissolve a passivating layer. The whole process is driven by the chemical energy of the oxidation of the metal. All three of the processes must occur for the cell to be maintained, and any one of them can be the rate-limiting process. This same electrochemical cell can drive dissolution in a pit, crevice, or at the bottom of a crack.

The electrochemical cell just described is quite simplified, as migration, reactions, and precipitation of metal ions and compounds all occur. However these cells will drive chloride into the pit, crevice or crack and also acidify the solution at the anode. As the local corrosion drives deeper into the metal, the anode at the base and the cathode at the surface become increasingly separated which can reduce the rate at which ions can be driven between them and thus the overall corrosion rate. However, the acidic, low potential, environment in a deep penetration may promote the other cathodic reaction, reduction of hydrogen ions to form hydrogen radicals or hydrogen gas. This can occur right at the anode and result in uptake of hydrogen by the metal and cause hydrogen embrittlement. This reaction will consume acid, so some continuation of an electrochemical cell with a remote cathode is required to maintain the local aggressive environment.

2.4.3 Cracking at the Tip

SSC only occurs when there is a tensile stress acting to help pull the crack open. The CGR has been found in most instances to depend on the stress intensity factor (K_I). As described by Jones (2003):

> "*Typically, three regions of crack propagation rate versus stress-intensity level are found during crack propagation experiments. These regions are identified according to increasing stress-intensity factor as stage 1, 2, or 3 crack propagation … No crack propagation is observed below some threshold stress-intensity level, K_{ISCC}. This threshold stress level is determined not only by the alloy but also by the environment and metallurgical condition of the alloy, and presumably, this level corresponds to the minimum required stress level for synergistic interaction with the environment. At*

low stress-intensity levels (stage 1), the crack propagation rate increases rapidly with the stress-intensity factor. At intermediate stress-intensity levels (stage 2), the crack propagation rate approaches some constant velocity that is virtually independent of the mechanical driving force. This plateau velocity, $V_{plateau}$, is characteristic of the alloy-environment combination and is the result of rate-limiting environmental processes such as mass transport of environmental species up the crack to the crack tip. In stage 3, the rate of crack propagation exceeds the plateau velocity as the stress-intensity level approaches the critical stress-intensity level for mechanical fracture in an inert environment, K_{Ic})."

SCC may be intergranular (along the grain boundaries) and/or transgranular. In sensitized material, intergranular corrosion and SCC is promoted.

There are many mechanisms proposed for the mechanical aspects of SCC but, as described by Jones (2003):

"[A] specific mechanism must attempt to explain the actual crack propagation rates, the fractographic evidence, and the mechanism of formation or nucleation of crack." "[The proposed mechanisms] usually assume that breaking of the interatomic bonds of the crack tip occurs by one of the following mechanisms:

- *Chemical solvation and dissolution*
- *Mechanical fracture (ductile or brittle)*

Mechanical fracture includes normal fracture processes that are assumed to be stimulated or induced by one of the following interactions between the material [at the crack tip] and the environment:

- *Adsorption of environmental species*
- *Surface reactions*
- *Reactions in the metal ahead of the crack tip*
- *Surface films*

All of the proposed mechanisms contain one or more of these processes as an essential step in the SCC process. Specific mechanisms differ in the processes assumed to be responsible for crack propagation and the way that environmental reactions combine to result in the actual fracture process."

Jones also discusses the most prominent models for SCC crack growth, which fall into two broad categories, dissolution models and mechanical fracture models:

- Dissolution Models
  - Film Rupture or Slip-Dissolution
- Mechanical Fracture Models
  - The Corrosion Tunnel Model
  - Adsorption-Enhanced Plasticity
  - The Tarnish Rupture Model
  - The Film-Induced Cleavage Model
  - Adsorption-Induced Brittle Fracture

– Hydrogen Embrittlement.

2.4.4 SCC steps

As stated by Jones (2003):

> *"The mechanisms that have been proposed for SCC require that certain processes or events occur in sequence for sustained crack propagation to be possible. These requirements explain the plateau region in which the rate of crack propagation is independent of the applied mechanical stress. That is, a sequence of chemical reactions and processes is required, and the rate-limiting step in this sequence of events determines the limiting rate or plateau velocity of crack propagation".*

The processes Jones identifies for aqueous SCC are paraphrased here for clarity:

- Mass transport of species from the cathode, down the crack, to the crack tip
- Reactions in the solution near the crack
- Surface adsorption of species at or near the crack tip
- Surface diffusion
- Surface reactions
- Absorption of species into the bulk metal
- Diffusion of species within the metal to the plastic zone ahead of the advancing crack
- Chemical reactions within the metal
- The rate of interatomic bond rupture

> *"Changes in the environment that modify the rate-determining step will have a dramatic influence on the rate of crack propagation, while alterations to factors not involved in the rate-determining step or steps will have little influence, if any. However, significantly retarding the rate of any one of the required steps in the sequence could make that step the rate-determining step. In aqueous solutions, the rate of adsorption and surface reactions is usually very fast compared with the rate of mass transport along the crack to the crack tip. As a result, bulk transport into this region or reactions in this region frequently are believed to be responsible for determining the steady-state crack propagation rate or plateau velocity."* (Jones 2003)

2.4.5 Parameters that May Influence the CGR in Aqueous Conditions

Depending on the step(s) that limit the CGR, the following environmental parameters are known to influence the CGR in aqueous solutions (Jones 2003):

- Temperature
- Solute species
- Solute concentration and activity
- pH
- Electrochemical potential
- Solution viscosity

In addition to these environmental parameters, stress-corrosion crack propagation rates are influenced by (Jones 2003):

- *The magnitude of the applied stress or the stress-intensity factor*
- *The stress state, which includes plane stress and plane strain*
- *The loading mode at the crack tip (tension or torsion, for example)*
- *Alloy composition, which includes nominal composition, exact composition (all constituents), and impurity or tramp element composition*
- *Metallurgical condition, which includes strength level, second phases present in the matrix and at the grain boundaries, composition of phases, grain size, grain-boundary segregation, and residual stresses*
- *Crack geometry, which includes length, width, and aspect ratio; and crack opening and crack tip closure*

2.5 Additional Processes Involved in the Possible Initiation and Propagation of SCC on UNF Canisters

In addition to the processes and important parameters for SCC under aqueous conditions described in Section 2.4, there are processes and parameters that are specific to atmospheric SCC. In atmospheric SCC, the aqueous solution is a thin brine film, and its dimensions may also influence the crack initiation and growth rates.. The dimensions shown to be important for some systems are the film thickness and if droplets, the drop area. These are determined by the following parameters: the composition of surface deposits, areal density and areal distribution of the salts on the surface, and the surface relative humidity (RH). The film thickness can influence all three electrochemical processes, anodic, cathodic, and ion transport. Tomashov (1964) suggested that the optimal film thickness for electrochemical corrosion is about 1 μm, which is 10 to 100 times thinner than can be seen by the naked eye. Above this value, the cathode resistance controls the rate and increasing brine thickness decreases the rate of O_2 transport to the metal surface. Below this value the rate switches from cathode control to anode control. Extremely low film thicknesses stifle all three processes as there is not enough water at the cathode to allow hydroxide formation, there is not enough water at the anode for metal ion hydrolysis, and there is insufficient water for effective ion transport. However, since Tomashov's report, Nishikata et al. 1997 have produced new data that show the optimal NaCl film thickness for corrosion of iron at 20 to 30 μm.

Thus to the list in Section 2.4.5 we add:

- Deposit composition
- Areal density of deposits
- Areal distribution of deposits
- Surface RH.

There is some debate over the importance and relevance to the SCC of UNF canisters of some the processes described above, due to lack of data specific to the range of conditions dry storage canisters will experience. In addition, the influence of many of these processes on CGR are codependent or synergistic, thus increasing the data needs for model development. This has contributed to the different lists of processes included in the models of SCC presented in Section 3 below.

2.5.1 Deposit Composition

2.5.1.1 Near Marine Environments

In near-marine settings, chloride-rich sea-salt aerosols constitute a significant fraction of the salt load in atmospheric aerosols, and will control the conditions at which deliquescent brines form on the canister surface. Thermodynamic modeling provides information on what salts precipitate when sea-spray evaporates to form sea-salt aerosols; these salts will ultimately control the deliquescence RH of sea-salts. The predicted evolution of the brine as seawater is evaporated at 25ºC was modeled by Bryan and Enos (2015a) using the thermodynamic solubility and speciation modeling program EQ3/6 (Wolery and Jarek, 2003) and the Yucca Mountain Program Pitzer database (SNL 2007), and is shown in Figure 2-1a.

As seawater evaporates, the composition of the remaining brine changes as different salt minerals precipitate, and in many cases, redissolve. On this plot, the concentration factor is the amount of water remaining in the brine, relative to the amount present in seawater; species that are conserved in the brine phase rise monotonically with degree of evaporation forming, diagonal lines across the plot. Inflections in the line occur when minerals precipitate or redissolve. The salts that precipitate and redissolve during evaporation are shown in Figure 2-1b. Comparing these two figures, the general trends in seawater composition with evaporation are illustrated and explained. Ca^{2+} is largely conserved in solution until gypsum ($CaSO_4$:$2H_2O$) precipitates at a concentration factor of about 3.7, and then it drops to low concentrations and remains there. Na^{+} is conserved until halite begins to precipitate at a concentration factor of 10.9, and then drops markedly with further evaporation; at this point, the brine is dominantly a magnesium chloride solution. Magnesium continues to increase monotonically until the first Mg-chloride containing phase (carnallite: $KMgCl_3$:$6H_2O$) precipitates at a concentration factor of about 115. At a concentration factor of about 222 (corresponding to an RH of about 35.6%), a stable suite of minerals begins to precipitate out, and concentrations of all species except for bromine and boron become fixed. The stable suite of minerals is (in order of abundance): halite (NaCl), bischofite ($MgCl_2$:$6H_2O$), kieserite ($MgSO_4$:$2H_2O$), anhydrite ($CaSO_4$), carnallite ($KMgCl_3$:$2H_2O$), and a very tiny amount of hydromagnesite ($Mg_5(CO_3)_4(OH)_2$:$4H_2O$).

Beyond this point, any changes in composition due to the continued build-up of bromine and boron, which are conserved in the brine phase through the entire run, until the code is no longer able to calculate a brine composition. Realistically, some phase containing these species would precipitate, limiting their concentration. However, the Yucca Mountain Pitzer database is not qualified for boron species, and, although qualified for bromine-containing brines, may not contain sufficient Br species to adequately model its behavior in very concentrated brines. A true deliquescent brine assemblage for seawater would have to include minerals containing these two species, for this reason, the deliquescence point described above (35.6% RH) may be high. However, because these species are present in very low concentrations in seawater (less than 100 mg/L), any brine formed below 35.6% RH due to their presence would be of extremely limited volume.

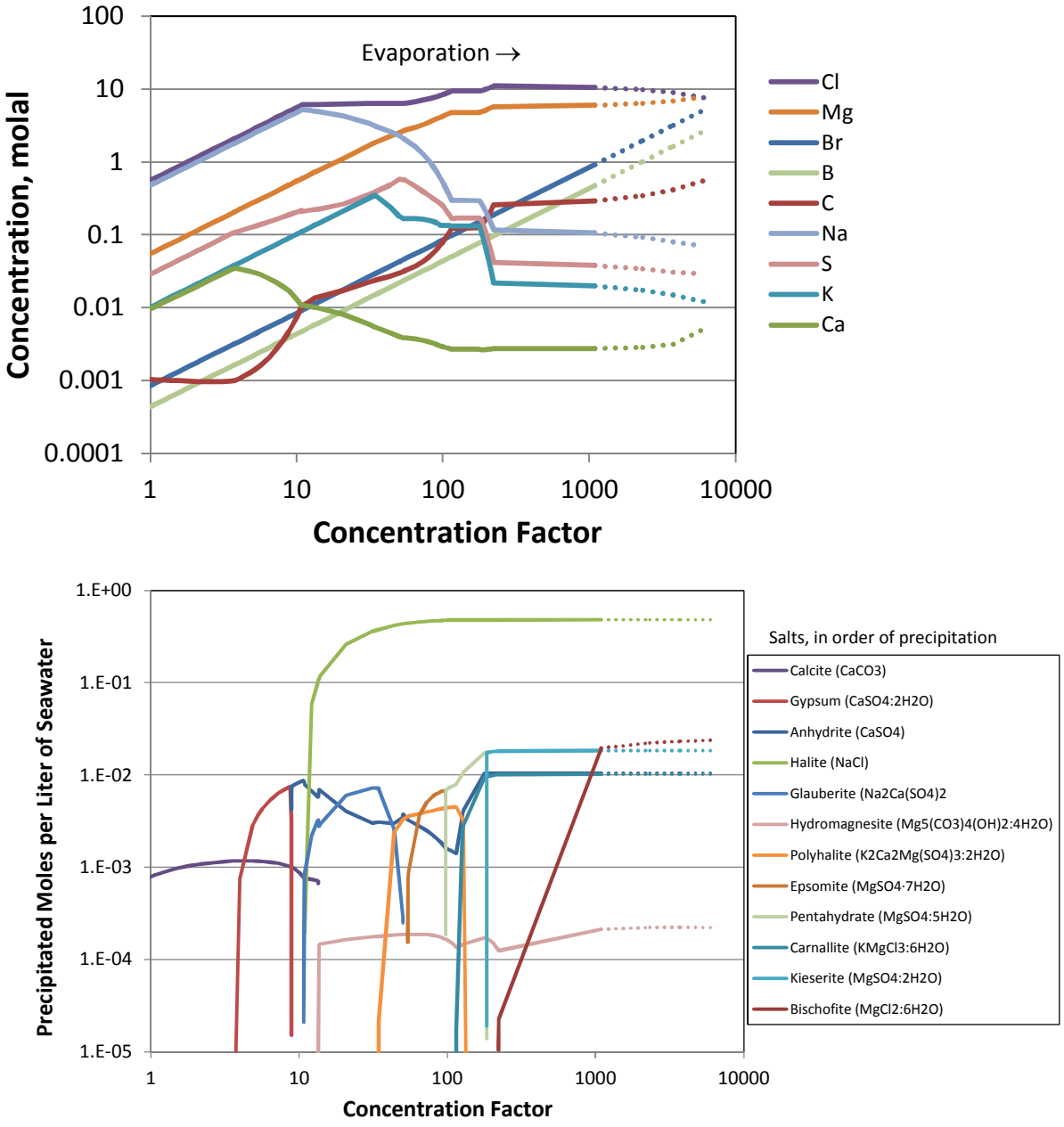

Figure 2-1. Evaporation of seawater. a) Predicted brine composition as a function of concentration factor. b) Predicted salt phases as a function of concentration factor.

2.5.1.2 Inland salt assemblages

Inland salt aerosols are dominated by ammonium minerals, including ammonium sulfate and smaller amounts of ammonium nitrate. Chloride concentrations are generally low, but chloride salts from road salting operations or from power plant cooling towers may result in locally high concentrations in the aerosols. Recent experimental work by Bryan and Enos (2015a) shows that chloride and/or nitrate cannot co-exist with ammonium in brine on an even mildly-heated canister surface. Hence, a chloride-rich brine

can only form if the rate of chloride deposition is large relative to that of ammonium. If this should occur, then the likely assemblage of salts on the surface would be the deposited chloride phase (presumably, NaCl or a $CaCl_2$ hydrate) and Na- and Ca-sulfates and possibly nitrates formed by reaction of the chloride salts with ammonium sulfate and ammonium nitrate, and with sulfuric and nitric acid in the gas phase. (Bryan and Enos, 2015a).

2.5.2 Accumulation of Sufficient Chloride on the Canister Surface

2.5.2.1 Is There a Chloride Density Threshold for SCC Initiation?

There has been debate over the importance of chloride surface density (CSD) to atmospheric SCC and whether there is a chloride surface density threshold (CSDT) on the canister surface below-which SCC will not initiate. Measured thresholds range from 2 g Cl/m^2 (304L with sea-salt at 70ºC and 15% RH, and tensile stress of 1.1 σ_y [312 MPa], Shirai et al. 2011a) to 0.005 g/m^2 (using NaCl and 304L SS at 50ºC, 50% proof stress, and 75% RH for about 1.6 years, Taylor 1994) and (using NaCl and sensitized 304 SS with cycling between 50-55ºC and 70-75% RH at 400 MPa for 60 days, Tokiwai et al. 1985) (see Table 2-1 below). Measured thresholds seem to be dependent on metal, sensitization, surface treatment, stress, salt composition, temperature, RH, and duration of experiment – the same parameters important to CGRs. For example, when Tokiwai et al. (1985) performed the experiment cited above but with the stress reduced by a factor of a little more than one half, the CSDT rose by 2 orders of magnitude.

The film thickness and chloride concentrations and CSD in solution for this range of CSDT are informative. The CSDT for 304L SS and NaCl at 75% RH between 50 and 90ºC of 0.005 g/m^2 equates to a film thickness of about 0.023 μm with a solution chloride concentration of about 6M. By comparison, sea-salt at 50ºC and 33% RH requires about 20 times the CSD (about 0.1 g/m^2) to obtain this film thickness and the solution chloride concentration would be about 10M and CSD in solution would be 0.009 g/m^2 . The CSDT obtained for these conditions provided by Shirai et al. (2011a) is 0.3 g/m^2.

The film thicknesses associated with measured CSDTs are all below the values where the resistance to oxygen migration to the metal surface is a factor in controlling the SCC rate. However, these thin films influence the electrical conductivity of the solution pathway between the anode and cathode. The amount of current carried by the solution depends on several competing factors including the film thickness and the concentration of mobile ions such as chloride. For a given salt loading, film thickness increases with RH but chloride concentration decreases. Tests measuring CSDT are normally conducted at RH values intended to maximize the film conductivity. The electrical resistance of the solution pathway increases with distance, which results in a limited cathodic area that may participate in the electrochemical cell. Thus on large surfaces, systems with thicker films and/or higher chloride concentrations have larger effective cathodic areas.

Of the CSDTs listed in the Table 2-1, the ones most relevant to SCC of DCSS canisters are those measured at the conditions closest to those expected at the ISFSIs when corrosion first starts. These are temperatures in the range of 50 to 60ºC and RHs in the range of 15 to 35%. The most relevant CSDTs are repeated in Table 2-2.

Table 2-1. Measured Chloride Surface Density Thresholds Shown in Order of Increasing Chloride Densities in Solution.

CSDT (g/m^2)	salt	CSD in solution (g/m^2)	[Cl] molar	brine thick-ness (µm)	SS	Sensi tized ?	Stress (MPa or % PS	T (°C)	RH %	days	reference
0.5	Sea-salt	0.0021*	7.1*	0.0084*	304L	no	312	60	25	42	Shirai et al. 2011a
0.005	NaCl	0.005	6.2	0.0228	304L	yes	50%	50 to 90	75	584	Taylor 1994
0.005	NaCl	0.005	6.2	0.0228	304L	no	50%	90	75	584	Taylor 1994
0.005	NaCl	0.005	6.2	0.0228	304	yes	400	50-55 (cycle)	70-75 (cycle)	60	Tokiwai et al. 1985 Fig. 4
0.01	NaCl	0.01	6.2	0.0456	304	yes	225	50-55 (cycle)	70-75 (cycle)	60	Tokiwai et al. 1985 Fig. 4
0.01	NaCl	0.01	1.0	0.2825	304	yes	400	50-55 (cycle)	95-98 (cycle)	60	Tokiwai et al. 1985 Fig. 3
0.3	Sea-salt	0.0269	10.0	0.0759	304L	no	312	50	35	42	Shirai et al. 2011a
0.03	NaCl	0.03	1.0	0.8475	304	yes	225	50-55 (cycle)	95-98 (cycle)	60	Tokiwai et al. 1985 Fig. 3
0.1	$MgCl_2$	0.1	10.6	0.2650	316L	no	U bend	50	33	84	Albores-Silva et al. 2011
0.25	$MgCl_2$	0.25	10.1	0.7000	316L	no	U bend	30	34	84	Albores-Silva et al. 2011
0.5	NaCl	0.5	6.2	2.2781	304	yes	180	50-55 (cycle)	70-75 (cycle)	60	Tokiwai et al. 1985 Fig. 4
1.6	$CaCl_2$	1.6	8.4	5.3668	304L	HAZ	300 to 400	50	30	56	Prosek et al. 2014

*at RH below about 30%, the concentration and brine thickness calculations are not reliable

Table 2-2. Measured Chloride Surface Density Thresholds at Relevant Conditions

CSDT (g/m^2)	salt	CSD in solution (g/m^2)	[Cl] molar	brine thick-ness (µm)	SS	Sensiti zed?	Stress (MPa or % PS	T (°C)	RH %	days	reference
0.5	sea	0.0021*	7.1*	0.0084*	304L	no	312	60	25	42	Shirai et al. 2011a
0.3	sea	0.0269	10.0	0.0759	304L	no	312	50	35	42	Shirai et al. 2011a
0.1	$MgCl_2$	0.1	10.6	0.2650	316L	no	U bend	50	33	84	Albores-Silva et al. 2011
1.6	$CaCl_2$	1.6	8.4	5.3668	304L	HAZ	300 to 400	50	30	56	Prosek et al. 2014

*at RH below about 30%, the concentration and brine thickness calculations are not reliable

2.5.2.2 Chloride Surface Density Modeling

The change in CSD with time depends on a balance of deposition rates and volatilization rates.

Deposition Rate

Chloride deposition rates are thought to depend on many factors including: chloride concentration within the air, air RH, air flow rate, geometry of air flow around the canister, angle of canister surface relative to horizontal, canister temperature, and time of exposure. It is expected that deposition rates will be site and canister-specific and will change with time.

Chloride Volatilization Rate

At both marine and inland ISFSI sites, many reactions can result in chloride loss from aerosol particles or deliquesced brines on the surface of UNF storage canisters. These reactions are reviewed in Bryan and Enos (2015a). Ammonium salts can decompose from the solid state, generating ammonia and a mineral acid. Ammonium chloride and ammonium nitrate, for instance, decompose so rapidly at even slightly elevated temperatures that they cannot accumulate or persist on the canister surface (Bryan and Enos, 2015a). Once an aqueous solution is present, either as a deliquescent brine or as an adsorbed water film, salts may react with gas phases in the atmosphere or with other salt phases. Some of these reactions can result in degassing of chloride and other anionic components as mineral acids, and loss of those species from canister surfaces. Possible exchange reactions with the atmosphere include acid degassing, equilibration with atmospheric CO_2, and coupled degassing of ammonia and acid gases. Degassing of HCl from a deliquesced brine is self-limiting (loss of acid caused the pH to rise, limiting further degassing), unless a balancing reaction buffers the pH. Balancing reactions include CO_2 adsorption and carbonate precipitation, precipitation of a hydroxide-containing phase (e.g., a $Mg(OH,Cl)_2:XH_2O$ phase), and ammonia degassing. However, many of these reactions are highly temperature-dependent, and may even reverse direction as the canister surface cools, absorbing acid gases.

In addition, particle-gas conversion reactions may occur, in which one acid gas species is adsorbed and a second is degassed. Well-known particle-gas conversion reactions include:

$$NaCl(s,aq) + HNO_3(g) \leftrightarrow NaNO_3(s,aq) + HCl(g)$$

$$2NaCl(s) + H_2O + \tfrac{1}{2}O_2 + SO_2(g) \leftrightarrow Na_2SO_4(s) + 2HCl(g)$$

Because of these reactions, as sea-salt aerosols in near-marine settings are blown inland, they become progressively enriched in sodium salts of nitrate and/or sulfate, originating from reactions on primary particles of sea-salt (Wall et al. 1988; Pio and Lopes, 1998; Malm et al. 2003). Sea-salts deposited on a canister surface and exposed to continuous airflow will be subject to the same conversion reactions. Analyses of dust deposited on canisters at two ISFSIs in the eastern US (EPRI 2014d; Bryan and Enos 2014, 2015b) showed evidence for these reactions, but it is not clear if they occurred prior to or after deposition of the aerosols onto the canister surface.

Assessing the importance of these reactions is complex and requires knowledge of ambient atmospheric acid gas and ammonia partial pressures. Developing a model to account for them has not yet been attempted.

2.5.3 Areal Distribution of Deposits

Deposited salt loads on canister surfaces are commonly described in units of grams/m^2. However, the salts will be present, at least prior to deliquescence, as individual grains. A very light salt load could represent an even coating of very small dust particles, or a few widely dispersed but large salt grains. In particular, sea-salts, which form by evaporation of sea-spray, tend to be coarse-grained. Sea-salt particles observed on the surface of in-service canisters at the Diablo Canyon ISFSI were on the order of 5-20 µm

in diameter. If single salt particles are sufficient to support SCC, then the concept of a chloride deposition threshold may be invalid.

Corrosion reactions have been observed associated with single grains of NaCl in the sea-salt size range (Schindelholz et al., 2014b), indicating that extremely limited brine volumes are capable of supporting corrosion. However, Schindelholz et al. evaluated mild steel, and 304 SS may not be so susceptible. Moreover, larger brine volumes may be required to support SCC as opposed to surface pitting; the ability to carry current from the cathode to the anode may be too restricted unless a continuous film is present. There is currently insufficient data to evaluate the importance of areal distribution of chloride on SCC initiation or growth.

2.5.4 Deliquescence of Salts and the Limiting RH for Corrosion

Deliquescence is defined as the process in which a salt absorbs water from the air and forms a solution. The relative humidity (RH) at which this occurs is called the deliquescence RH (DRH), and corresponds to the point at which the activity of water in the air (the RH in unit form) is equal to the activity of water in a solution that is saturated with the salt, or salt assemblage, in question. The reverse process, where a solution gives up its water and salt precipitates, is called efflorescence and occurs at the efflorescence RH (ERH). Because a nucleation energy barrier must be overcome for recrystallization to occur, the salt does not crystallize until a critical supersaturation is reached, which causes the ERH to be somewhat lower than the DRH. However, because formation of a stable crystallite is a stochastic process, the ERH will approach the DRH over time, although brine may persist in a metastable condition for a significant time at RH values below the DRH (for example up to 24 hours in Schindelholz et al., 2014a). The RH value at which deliquescence occurs is a property of the salt or salt mixture, and generally decreases slightly with increasing temperature. The DRH of salt mixtures must be lower than that of the constituent salts.

The limiting RH for corrosion (RH_L) is commonly below the deliquescence RH. Deliquescence is a property of the bulk salt that describes thermodynamic equilibrium between a salt saturated solution and the air. However, water adsorbs onto salts as surface films well below the deliquescence RH, and these films are sufficient to support corrosion and even stress corrosion cracking.

2.5.4.1 Deliquescence of Sea-salts

Section 2.5.1 discusses the salt assemblage that forms when sea-spray evaporates to form sea-salt aerosols. Based on thermodynamic modeling, the predicted salt assemblage is (in order of abundance): halite (NaCl), bischofite ($MgCl_2{:}6H_2O$), kieserite ($MgSO_4{:}2H_2O$), anhydrite ($CaSO_4$), carnallite ($KMgCl_3{:}2H_2O$), and a very tiny amount of hydromagnesite ($Mg_5(CO_3)_4(OH)_2{:}4H_2O$). Predicted deliquescence behavior as a function of temperature for the individual salt minerals of the final assemblage and for mixtures of them is shown in Figure 2-2. Some previous work (He et al. 2014a) has suggested that highly deliquescent $CaCl_2$ plays an important role in determining the deliquescence of sea-salts, depressing it relative to hydrated magnesium chloride phases. However, this is unlikely to be true, as calcium is removed from the evaporating brine as sulfate, and calcium sulfate (either gypsum or anhydrite) is relatively low solubility, with a deliquescence RH of 99.9%. Mg-sulfate (3 different hydrates over the temperature range of interest) are moderately deliquescent, forming a brine between 94% and 84% RH. Halite deliquesces at ~76% RH. Carnallite deliquesces at 55%-49% RH (but when evaluated as a single salt, actually co-precipitates with sylvite (KCl) over part of the temperature range. Bischofite is the stable Mg-chloride hydrate over the entire temperature range and deliquesces at 37% to 29% RH (for respectively, 20ºC and 80ºC) over the temperature range shown. Mixtures of salts deliquesce below the DRH of any individual salt; for instance, mixtures of NaCl and Mg-SO_4 hydrates have DRH values well below the individual salts. However, because magnesium chloride has a much

lower deliquescence RH than the other salts present, it largely controls the DRH of mixtures containing it, and the predicted values are only slightly lower than the value for Mg-Cl_2 alone (Figure 2-2).

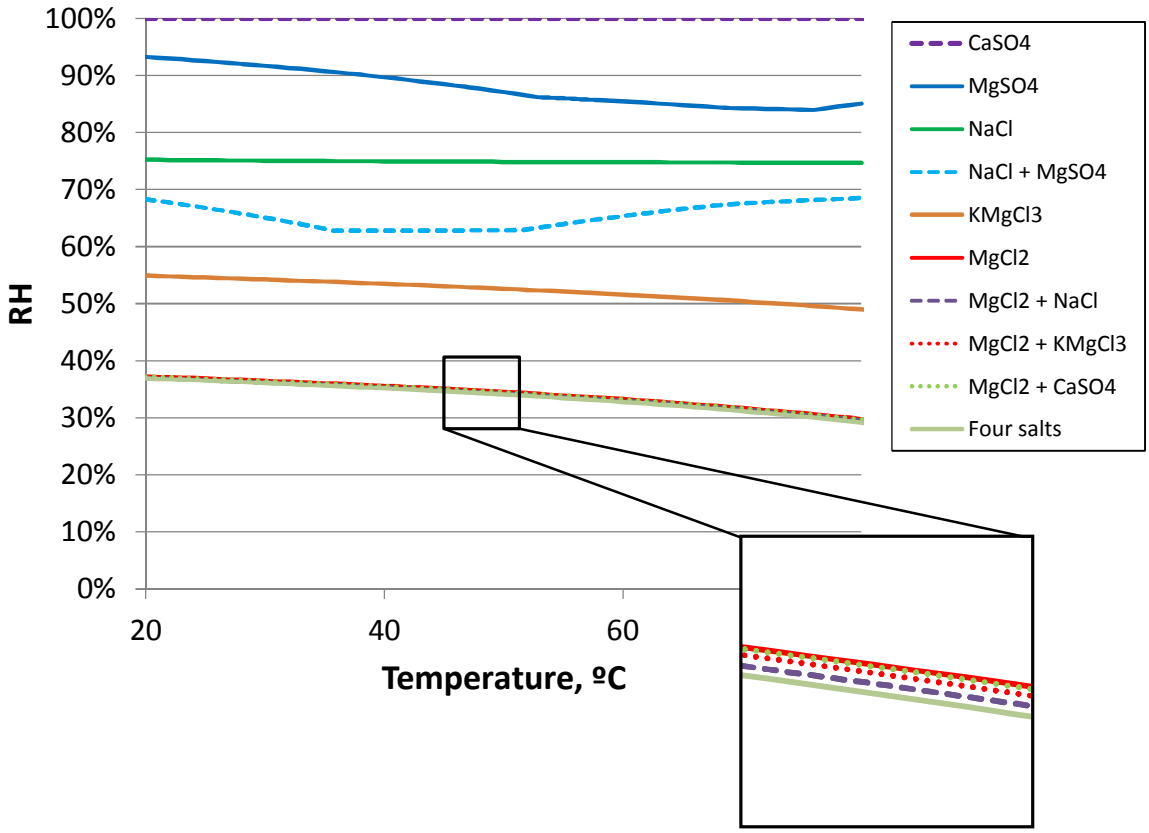

Figure 2-2. Predicted deliquescence behavior of salts that precipitate when seawater is evaporated (note that chemical formulas do not include waters of hydration).

It should be noted that He et al. (2014a) conducted deliquescence tests with artificial mixtures of salts representing sea-salts and saw DRH values 5% to 10% lower than for $MgCl_2$ alone. However, the salt assemblage used was that used to mix synthetic sea-water, not what is produced when seawater evaporates. It included phases such as Na_2SO_4 and highly-deliquescent $CaCl_2$ neither of which forms when seawater is evaporated. While these phases should have reacted upon deliquescence to produce non-deliquescent $CaSO_4$, slow dissolution of the Na_2SO_4, or poor mixing of the salt assemblage, may have limited the reaction and allowed the $CaCl_2$ to control deliquescence.

RH_L for sea-salt

As noted previously, RH_L is the relative humidity at which corrosion can occur, and is generally somewhat below the deliquescence RH for the salt assemblage. Sea-salts are generally considered to deliquesce at ~30% RH, but corrosion has been observed on metal coupons covered with sea-salts at RH values well below this value. Because corrosion below the deliquescence RH is due to adsorbed water films which do not exhibit the thermodynamic properties of bulk solutions, it is not possible to assess the RH_L using thermodynamic modeling. However, several experimental studies have observed adsorbed water on sea-salt minerals, and have observed corrosion reactions occurring at values below the

deliquescence RH. Dai et al. (1997) observed the adsorption of water onto surfaces of NaCl below the deliquescence point (DRH ~77%), concluding that a continuous water film formed at relative humidities down to 35%, and discontinuous sorption (primarily at step edges) occurred at even lower RH values. That such water films could support corrosion reactions was demonstrated by Schindelholz et al. (2014b), who cites several studies that observed corrosion of mild steel by deposited NaCl at RH values of 50% to 58%; their own 21ºC study showed corrosion as low as 33% RH. They also noted that once corrosion initiates, it can persist down to even lower RH values (at least 27% RH) due to the presence of highly deliquescent iron chloride salts. Schindelholz et al. (2014c) repeated the experiments with hydrated $MgCl_2$ (DRH~33%) and observed corrosion as low as 11% RH, at relatively light salt loadings of 80 mg/m^2. When sea-salts were used, corrosion was observed as low as 33% RH at a loading of 16 mg/m^2; however, at a higher loading of 1.6 g/m^2, corrosion occurred as low as 23% RH. Schindelholz et al. (2014c) inferred that at RH values below the DRH for $MgCl_2$, sea-salt corrosion behavior was largely controlled by $MgCl_2$, but because only a small fraction of the total deposited salts were $MgCl_2$, a significantly larger load of sea-salts are required to result in corrosion, and to result in the same rate of corrosion. These results are very important, because they imply that the RH_L for corrosion is a function not only of the composition salts present, but also of the surface loading of salts and the total amount of the chloride that is present in brine rather than as solid salts. At low RH, a small surface load of sea-salt is not corrosive because there is an insufficient amount of brine to support a corrosion reaction; however, a larger amount of sea-salt at the same RH will result in corrosion. Conversely, as the RH increases and a larger fraction of the sea-salts deliquesces, then corrosion can occur even with a very small sea-salt surface load because a larger fraction of it is in solution. In short, the RH_L decreases as the salt load increases.

Studies with 304 SS have been less thorough, but similar trends have been documented, shown specifically to apply to SCC initiation. He et al. (2014a) observed SCC formation in samples of sensitized 304 SS in 60ºC tests that cycled the RH from 12%-23%, and observed SCC of both sensitized and unsensitized 304 SS samples in tests at 60ºC and a fixed RH of 25%. Corrosion at the lowest RH values corresponded to the samples with the heaviest salt loads, while lighter sea-salt loads were only corrosive at higher RH values. Mayuzumi et al. (2008) observed corrosion of 304 SS at 80ºC in a system with an RH that changed over time from 16% to 20%. The lowest RH value at which SCC of 304 SS has been observed is ~15% (Fairweather et al., 2008; Shirai et al., 2011a). Shirai et al. observed SCC at 70ºC and 80ºC; at both temperatures where the absolute humidity (AH) required to achieve 15% RH is higher than occurs under natural conditions. However, Fairweather et al. observed SCC at 60ºC and 45ºC and 15% RH, corresponding to AH values that are within the range observed in nature. While these data confirm that the RH_L is a function of salt load, a systematic study of the relationship between the two has not been carried out, and cannot be applied to predict the occurrence of SCC at this time.

2.5.4.2 Inland Salts

As discussed in Section 1, chloride brine may not persist at many inland sites because of reactions with ammonium minerals. However, if excess chloride relative to ammonium is deposited, then a brine could form. The likely salt mineral assemblage would be Na-, Ca-, and K-containing chloride and sulfate phases, with some nitrate. Because chlorides are generally much more soluble than sulfates (the most soluble sulfates, $MgSO_4$ hydrates, are unlikely at inland sites), the deliquescence behavior of these salts would likely controlled by the chloride phase, and the nitrate phase if present. An estimate of deliquescence conditions would require more information than is currently available.

3. PREDICTING SCC - AN OVERVIEW OF SOME RECENT SCC MODELS AND THE SIMPLIFYING ASSUMPTIONS MADE

In Sections 3.1.1 through 3.1.3, three recent modeling efforts are reported without comment on the decisions and simplifications made during the model development. A summary table is provide in 3.1.4. Due to limited and conflicting data, these decisions and simplifications are not straight-forward and thus there are many differences between the models. The limitations and the strengths of the technical justifications behind each model are discussed in Section 3.2. Areas in which the models differ point to unresolved issues that greatly increase the uncertainty in the predictions made by these models. These issues and resulting uncertainty are discussed in Section 3.3. Section 3.4 provides a summary of the state of uncertainty in SCC prediction.

3.1 Model Overviews

3.1.1 CREIPI

CRIEPI has been studying SCC of austenitic steels since at least 1985 when Tokiwai et al. (1985) published results of an investigation on the minimal amount of chloride that would support SCC on 304 SS. Much of this literature is in Japanese, but Shirai et al. published an overview in English in 2011. This summary is based on that report. Shirai et al. (2011a) described the progression for SCC from chloride deposition, deliquescence, rust formation with pits or crevices, SCC initiation, and crack growth. In their mitigation section they provide data on the times to crack failure versus applied stress under extreme conditions.

3.1.1.1 Chloride Deposition

Based on field and laboratory tests, CRIEPI created the following empirical chloride deposition model.

$$Q = \{5.07 - 0.022(T - 30)\} \cdot (1.55\, t \times C/10000)^{0.5} \quad \text{Eq. 3-1}$$

where Q is the amount of salt deposition (mg/m^2 as Cl), t is time (hours), C is the airborne chloride concentration (µg/m^3 as Cl), and T is the canister surface temperature (°C).

Based on calculations of the temperature of the canister bottom within the concrete cask (the CRIEPI model only evaluated SCC at a single location on the canister), the following equation for temperature was obtained.

$$T = -0.575X + 89 \quad \text{Eq. 3-2}$$

where X is time in years from emplacement.

With these two equations, the amount of salts deposited on the surface can be calculated as a function of time.

3.1.1.2 Deliquescence

The absolute humidity is obtained from weather data, with an example from the east-central coast of Japan from 1991 to 2003. From the weather data, and the temperature from the above equation, the surface RH is calculated. With an RH_L of 15%, the time when $RH \geq RH_L$ was calculated as 15000 hours (1.7 years) in 60 years, at the canister bottom location evaluated.

3.1.1.3 SCC Initiation

Estimates of the threshold chloride density for rust initiation and SCC initiation were determined experimentally, using data from four test conditions. The chloride was deposited using simulated sea water spray and the following conditions were tested: 50ºC-35% RH, 60ºC-25% RH, 70ºC-15% RH, and 80ºC-15% RH. The tensile stresses and durations of these tests were not specified, but examination of the figures in their reports shows the sample from the 304L SS 50ºC-35% RH test at 10 g/m^2 as Cl, with a tensile stress of 1.1 σ_y, and a duration of 1000 hours. The lowest thresholds were seen in the 50ºC-35% RH test with a rusting chloride threshold of 0.1 g/m^2 and an SCC chloride threshold 0.3 g/m^2.

Using the equations from 3.1.1.1 and their reported typical airborne concentration of 16 $\mu g/m^3$ as Cl at 400 m from the sea, the chloride density at 60 years would be only 0.16 g/m^2.

3.1.1.4 Crack Growth

Crack depth data collected by CRIEPI showed two phases of growth, an initial fast rate to about 2 mm depth followed by a much slower rate. This test was run for almost a year on 304L SS at 80ºC, 35% RH, 270 MPa, and 10 g/m^2 as Cl of sea-salt. It was noted that when $MgCl_2$ was used, only the fast rate was seen. The conditions of the sea-salt test can only be achieved with an absolute humidity much greater than seen in nature, and thus were very conservative compared to that expected on storage canisters. The slope of the curve during the slow growth phase for the test shown was 7.6×10^{-12} m/s. The value chosen for use in the Shirai et al. (2011a) report was 1×10^{-11} m/s (0.32 mm/year). When combined with the amount of time $RH \geq RH_L$ in 60 years, a penetration of 0.5 mm is calculated. Note this penetration depth demonstration was based on a CSD of 10 g/m^2. However, as previously noted, their chloride deposition equations predict that there would be insufficient chloride density on vertical surfaces within that time period for any SCC.

3.1.1.5 Stress

In the CRIEPI discussion of mitigation, they provide data on the times to crack failure versus applied stress for steels under extreme conditions: 10 g/m^2 chloride from sea-salt, 80ºC and 35% RH. The 304L SS samples were 2 mm thick, 5 mm wide, and 30 mm long. There was significant spread in the time to failure for each stress level, but the earliest times to failure for 304L SS ranged from about 240 hours at about 500 MPa to about 425 hours at about 150 MPa. However even at about 500 MPa, there were samples that did not fail in 1000 hours. Both as-machined welded samples and samples with surface treatments were used, and stresses were mostly near 250 MPa, with one data point at about 500 MPa.

3.1.2 EPRI

This section is based on the description of the CGR model provided in the Flaw Growth and Flaw Tolerance report (EPRI 2014c).

3.1.2.1 Crack Growth Rate Equations

As stated in this report

> "*A review of literature* [EPRI 2014a] *did not identify an established crack growth relation for CISCC at temperatures below 100ºC or in atmospheric conditions. In order to quantify the rate of atmospheric CISCC propagation, a new CGR equation is developed in this report. The CGR equation is based upon the typical form of SCC flaw propagation, such as those found in Section XI Nonmandatory Appendix C, Article C-8000, of the ASME Boiler and Pressure Vessel Code.*

The crack growth rate formula includes an Arrhenius relation to describe the thermal dependence and additional factors to describe other dependencies."

The primary factors considered were: the stress intensity factor, the surface temperature, the ambient humidity, the chloride areal density, the crack depth, and the material alloy. These were evaluated in their Appendix A with the following conclusions: 1) the canister surface temperature, the ambient humidity, and the crack depth are very important to the CGR and data is available to model them, 2) the dependency of the CGR on stress intensity factor was judged to be too weak to warrant modeling, 3) although important to CISCC, there is insufficient data to parameterize the effects of chloride areal density and alloy, 4) the remaining factors - material condition (e.g., sensitization, cold work, etc.) and presence of other species in the aqueous layer of deliquescent brine - are considered only so far as they were included in the underlying data used to determine the crack growth rate coefficient.

The final equations they developed were provided below (EPRI 2014c, Eq. 3-3, 3-4, 3-5, and 3-6):

$$CGR = \frac{da}{dt} = \begin{Bmatrix} \alpha\, exp\left[-\frac{Q_g}{R}\left(\frac{1}{T(t)} - \frac{1}{T_{ref}}\right)\right] & for\ RH\ \geq DRH\ and\ K_I > 0 \\ 0 & for\ RH < DRH\ or\ K_I\ \leq 0 \end{Bmatrix} \quad \text{Eq. 3-3}$$

where:

$\frac{da}{dt}$ = crack depth growth rate

α = crack growth rate coefficient (mm/yr), which is the CGR at the reference temperature (T_{ref})

$$= \begin{Bmatrix} 168\,\frac{\text{mm}}{\text{yr}} \text{ for a} < 3.16 \text{ mm}^{b} \\ 2.2\,\frac{\text{mm}}{\text{yr}} \text{ for a } \geq 3.16 \text{ mm} \end{Bmatrix} (T_{ref} = 80^{\circ}\text{C})$$

Q_g = crack growth activation energy (kJ/mole) = 40 kJ/mole

R = universal gas constant (kJ/mole/K) = 0.008314 kJ/mole/K

T = surface temperature (K), obtained by measurement or analysis using Equation 3-5

T_{ref} = Arrhenius reference temperature (K) = 353.15 K (80ºC)

RH = local relative humidity at the canister surface (%), obtained from surface temperature and ambient absolute humidity using Equation 3-6

DRH = deliquescent relative humidity of deposited chloride salts (%), from Equation 3-4

$$\text{DRH}(T) = 0.01\,[33.67 - 7.974\times10^{-3}\,(T\text{-}273.15) - (1.090\times10^{-3}\,(T\text{-}273.15)^2] - \Delta_{\text{offset}} \quad \text{Eq. 3-4}$$

$$T(t) = T_{offset}(t) + \int_{t-X}^{t} T_{atm}\,(\beta)d\beta \quad \text{Eq. 3-5}$$

$$RH(T) = \frac{(T)AH}{216.68}\, 10^{-23.5518 + \left(\frac{2937.4}{T}\right)} T^{4.9283} \quad \text{Eq. 3-6}$$

As described in (EPRI 2014c),

"[Equation 3-5] *above uses the dummy variable β to calculate the moving average of the atmospheric temperature (T_{atm}) over time X. This moving average, used to represent the canister's thermal inertia, is offset by T_{offset} to account for the canister thermal power to calculate the surface temperature. The*

[b] These crack growth rates and transition depths were obtained from a conservative statistical treatment of the data and have been reported to three significant digits. This precision is greater than is justified by the data, but is sufficient for these purposes.

surface temperature is then used to determine the local relative humidity and DRH in [Equations 3-6 and 3-3]. *In the above equations, T_{atm} and AH are defined by the climate data (hourly data is preferred) at or near a given site and T_{offset} is defined by either measurement or thermal analysis of the canister.*"

From the text, it appears that Eq. 3-6 is from Parish and Putnam (1977).

3.1.2.2 Important Parameters

The specified parameters in the above equations are α, the crack growth rate coefficient at 80ºC for the two phases of crack growth, the depth of transition from phase 1 to phase 2, the activation energy, and the DRH offset.

Crack Growth Rate Coefficient for the Two Phases of Crack Growth, the Depth of Transition from Phase 1 to Phase 2

These were obtained by applying a conservative statistical treatment to the data from Tani et al. (2009) and Shirai et al. (2011b). The shallow cracking data (phase 1) from the two references that met the EPRI criteria for inclusion were used. For deep cracking (phase 2), the data set from Shirai et al. (2011b) were used. Due to the small dataset (3 data points for the phase 2 CGRs; see Table 3-3 below), the log-normal fit to the data is obtained using the upper limit of the 50% confidence interval on the mean, and the 95th percentile value of this revised fit is used as the CGR coefficient. For the transition depth, a similar treatment was used except a normal fit to the data was used. The conservatism of this statistical approach may be seen by comparing the transition depth used, 3.16 mm, with those upon which it was based, ~1.7, 2.0 and 2.7 mm (see Table 3-3 below).

Activation Energy

There is a wide range in activation energies in the literature. The 40 kJ/mol activation energy was chosen from the lower end of the range of values to be conservative with the use of a high reference temperature.

The DRH Offset

The DRH Equation 3-4 is the one developed by Greenspan (1997) for $MgCl_2$, modified by an offset value of 7% to capture the lower bound of the results by He et al. (2014a). This is shown Figure 3-1 along with the Greenspan (1977) DRH for NaCl and $MgCl_2$, and the data for sea-salt DRH and ERH determined by He et al. (2014a) using an impedance method and visual observations of sea salt in beakers. This approach bounds most, but not all, of the available data. For instance, SCC in 304 SS observed at 15% RH by Fairweather et al. (2008), at 60ºC and 45ºC, is not captured by this assumption.

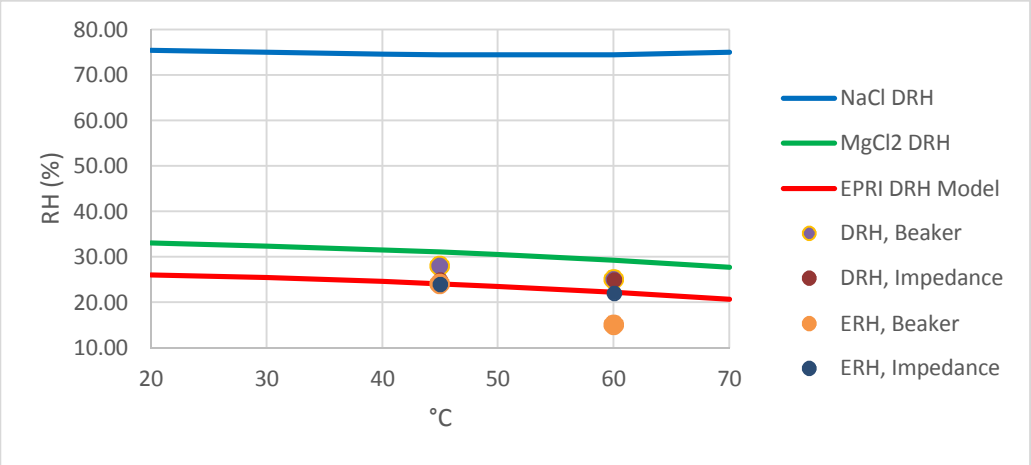

Figure 3-1. DRH Models by EPRI (EPRI 2015c), Greenspan (1977), and sea salt data by He et al. (2014a).

3.1.2.3 Application of the Model

To exercise the CGR equations, two sets of inputs were used: 1) hourly temperature and dewpoint data from seven locations in the US, including locations at the Pacific coast, the South Atlantic coast, the Mid-Atlantic coast, the arid South West, the Mid-West far from the ocean obtained from the National Oceanic and Atmospheric Administration (NOAA), and 2) T_{offset}, the difference between the canister surface temperature and the ambient temperature. The report does not try to model the temperature distribution across the canister but instead calculates the CGR for T_{offset} ranging from 0 to 35ºC. For sensitivity calculations, the time for through wall crack growth was determined with the initial T_{offset} set at 35ºC, 25ºC, and 15ºC. The T_{offset} is assumed to be proportional to the power which is decayed using a generic power decay curve for 24 assemblies: 10 assemblies of 40 GWd/MTHM after storage for 10 years and 14 assemblies of 30 GWd/MTHM after storage for 15 years, with a total decay heat of 12.2kW about a decade after discharge from the reactor. Unless otherwise stated, a T_{offset} of 25ºC was used. The sensitivity calculations were predominantly performed for two locations, the South East represented by the weather data from Homestead Air Force Base, and the West Coast represented by the weather data at Camp Pendleton. The assumed canister thickness was 0.5 inches. The sensitivity cases and the effect of parameter modifications on the predicted through-wall cracking time are listed in Table 3-1; each is a variant of the baseline cases, which are represented by cases 2 and 5.

Table 3-1. EPRI Sensitivity Cases

Case	ISFSI Location	Sensitivity Case	Time to Grow TW, (yr)
1	South East	Initial T_{offset} = 35ºC	41
2	South East	Initial T_{offset} = 25ºC	26.5
3	South East	Initial T_{offset} = 15ºC	30.9
4	West Coast	Initial T_{offset} = 35ºC	81.3
5	West Coast	Initial T_{offset} = 25ºC	63.2
6	West Coast	Initial T_{offset} = 15ºC	61.7
7	2nd South East	Initial T_{offset} = 35ºC	32.3
8	South East	Weather based on 4 years of climate data	27.3
9	South East	the 95th percentile value of the log-normal distribution that is the best-fit to the CGR coefficient datasets rather than that of the revised fit	84.3
10	South East	E_a = 30 kJ/mol	18.6
11	South East	E_a = 80 kJ/mol	>120
12	West Coast	E_a = 30 kJ/mol	38.9
13	West Coast	E_a = 80 kJ/mol	>120
14	South East	Fast-slow crack growth transition at 6 mm	19.1
15	South East	Shell thickness 0.625”	35.6
16	South East	DRH offset = 10%	22.1
17	South East	DRH offset = 4%	33.5
18	West Coast	DRH offset = 4%	75.6

3.1.3 SNL

SNL has been developing a probabilistic model for evaluation of UNF storage canister penetration by SCC. Although the parent report (Dingreville et al. 2014) is not publically available yet, the model is summarized in Bryan et al. (2015) and Appendix F of ORNL (2015). The model description provided here is taken from those reports, but also includes a description of ongoing model development efforts.

The SNL SCC model evaluates the environmental conditions on the storage canister surface as a function of location on the surface and time, and determines when the environmental conditions at a given location support localized corrosion. Then, corrosion is initiated, first as a pit because experimental and observational studies have shown that SCC cracks initiate from corrosion pits, and then transitioning into a stress corrosion crack. Pit and crack growth rates are a function of the environment, and are calculated for each location at each time interval. As discussed elsewhere in this report, the performance failure criterion is the development of a through-wall crack. Predicted SCC depths were tracked at different locations on the canister surface until penetration is predicted to occur, or for the first 100 years of storage, whichever occurs first. As a probabilistic model, the SNL model samples parameter values, with uncertainty, once per realization, and uses them to estimate SCC penetration times. A total of 200

realizations are run, providing a suite of results that are evaluated using statistical methods to determine the relative importance of parameters and parameter uncertainties. The model is intended to be used as a tool to identify parameters for which uncertainty has a large effect on predicted SCC penetration times. Reducing the uncertainty in such parameters will result in more accurate predictions of canister performance with respect to SCC.

Three different criteria are required for SCC of interim storage canisters: a susceptible material, a corrosive environment, the presence of sufficient tensile stress to support SCC; moreover, the tensile stress must exist through the entire thickness of the canister wall. The probabilistic model developed by SNL assesses whether these criteria are met at locations on the surface of storage canisters, and if they do, then it initiates corrosion and tracks crack growth through time until penetration occurs. It consists of several submodels for the environment at a given location on the canister surface, the through-wall tensile stress profile, corrosion pit initiation, pit growth, SCC initiation from pits, and SCC crack growth. There is no model for material susceptibility; the canisters are made of materials known to be susceptible (304 SS and 316 SS), and too little is known to include the effects of factors affecting susceptibility (Section 2.1). Instead, it is assumed that the experimental data used to parameterize the crack growth model, which were collected with a range of materials (sensitized, unsensitized, weld metal, etc.) capture the effects of variability in susceptibility.

3.1.3.1 Environment Model

The environment at any given location on the storage canister surface will be aggressive if two criteria are met: a corrosive chemical species is present, and aqueous conditions exist. For this model, the aggressive species is assumed to be chloride. It is also assumed that persistent aqueous conditions on the canister surface can only occur by deliquescence of dusts on the package surface. Advective flow onto the canisters is possible; water stains have been observed on canister surfaces during in-service inspections (EPRI 2014d), indicating that water may be blown into the outlet vents of the overpacks and drip onto the canisters. However, any advective flow of water onto the packages is likely to be transient because the storage canisters are hot relative to outside temperatures, and any water advecting onto the canister will rapidly evaporate. Hence, only deliquescence can result in long-term aqueous conditions on the canister.

As discussed in Section 2.5.2.1, a third potential criterion for a corrosive environment may be the amount of chloride present. Several studies (Shirai et al. 2011[a], Albores-Silva et al.2011, He et al. 2014a, Tokiwai et al. 1985, Taylor 1994, Fairweather et al. 2008) have shown that there may be a lower limit on the amount of chloride on the package that can support SCC initiation—however, these limits are low, ranging from 0.3 to 0.005 g/m^2. The United Kingdom Nuclear Decommissioning Authority (NDA) has issued cautious operational limits for chloride surface concentrations on 316L SS waste packages of 0.01 g/m^2 for temperatures between 10 and 30ºC and 0.001 g/m^2 for temperatures between 30 and 50ºC (NDA 2012). Given these low values, it is unlikely that low chloride surface load will effectively limit the initiation of SCC, and no chloride surface load was assumed to be necessary.

It is also possible that continued SCC growth after initiation is a function of the surface salt load, because it affects the current carrying capacity of the brine layer and the ability of the cathode, outside of the crack, to support corrosion at the anode, within the crack. This approach has been proposed for estimating maximum pitting penetration depths in several recent papers (Chen and Kelly 2010, Woldemedhin and Kelly 2014, Krouse et al. 2014) but has never been applied to SCC.

Presence of Chloride

The greatest concern of SCC is at near-marine sites, so the assumption is made in the SNL model that the deposited salts are chloride-rich sea-salts. It is known that sea-salts will deposit on canisters at some near-marine ISFSIs; aggregates of sea-salts were observed in dusts collected from in-service storage

canister surfaces at Diablo Canyon, on the California coast (Bryan and Enos 2014). It is also assumed that the salts are present immediately upon canister emplacement into storage, and that the rate of chloride loss due to degassing and particle-gas conversion reactions is less than the rate of deposition. Therefore, conditions for localized corrosion of the canister surface are assumed to occur any time that aqueous conditions are predicted to be present.

Aqueous Conditions

As discussed in Section 2.5.4, deliquescence occurs when the activity (chemical potential) of water in the atmosphere is equal to the activity of water in a saturated solution of the salt (or the salt assemblage) on the canister surface. The activity of water in air is equal to the RH expressed as a unit value, and the RH at which deliquescence occurs is the DRH. However, a bulk aqueous solution is not required for corrosion. An adsorbed water film is sufficient, and experimentally, corrosion is commonly observed at an RH significantly lower than the DRH, known as the limiting RH, or RH_L (Section 2.5.4). At any given point on the canister surface, corrosion can occur, or progress, if the location- and timestep-specific RH is greater than the RH_L. The derivation of canister surface location-specific RH values, and the value for RH_L, is described below. In order to identify the surface locations to evaluate, a weld-location model was also developed—SCC can only occur where there is sufficient tensile stress, and that condition is only likely to occur near welds.

Location-Specific RH on the Canister Surface

The location-specific RH values can be calculated from two parameters: the canister surface temperature at any given location; and the absolute humidity (AH), or water content, of the inflowing air.

Canister surface temperature—To determine location-specific canister surface temperatures through time, maps of canister surface temperatures were calculated using a specific set of parameter values for storage system design (horizontal); the fuel loading (number and geometry of assemblies); the fuel burnup; the heat load (corresponding to a given time out of reactor), and a single fixed ambient external temperature. The parameter values used are described elsewhere (Suffield et al. 2012). Decay heat loads were varied to represent waste emplaced into dry storage at different times out of the reactor. However, a single curve for heat generation as a function of time-out-of reactor, corresponding to a single fuel burn-up, was used. Hence, variations in fuel burnup are not considered.

The thermal modeling provided temperature maps of the canister surface for each of 8 decay heat loads corresponding to different lengths of time out of the reactor, for a single ambient temperature of 15.6ºC (60ºF) (for example, Figure 3-2). To abstract this for the SCC model, canister surface temperatures for each decay heat load were extracted at 35 positions on the canister surface. By interpolating between those c, the temperature at any point on the canister surface was estimated for a given decay heat load. To obtain the surface temperature at any location as a function of time, interpolation was done between temperature maps representing different heat loads (times out of the reactor).

The SCC model time-step was one day. Daily mean ambient temperatures for the simulation period of 100 years were calculated by sampling from a distribution fitted to one year of measured data from a relevant NOAA weather station. Then, the difference between the predicted ambient temperature and the nominal ambient temperature used in the thermal modeling (15.6ºC) was applied as a delta to the surface temperatures provided by the canister thermal model. This yielded the temperature used in that time step of the SCC model, for the location of interest on the canister surface.

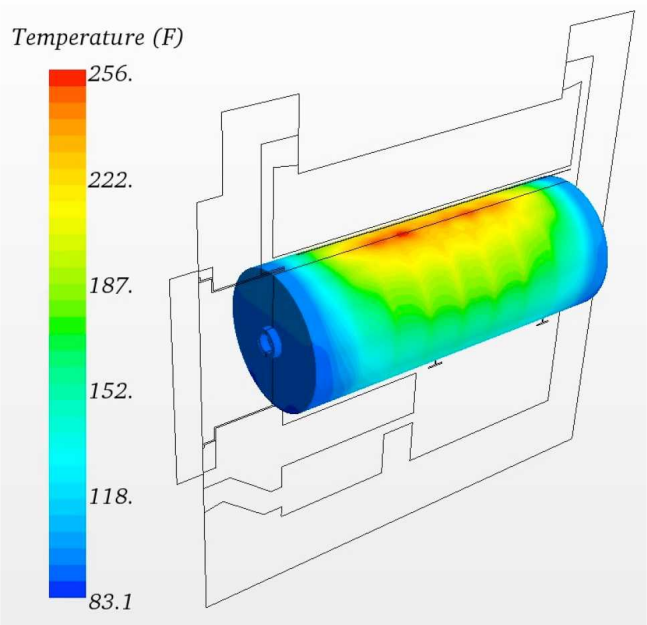

Figure 3-2. Canister surface temperature map, for a decay heat load of ~7.6 kW (Suffield et al. 2012).

Absolute humidity—Similarly to the ambient temperature, the predicted AH is based on one year of NOAA data from the same weather station. Based on the measured NOAA data, the predicted offsets for the ambient temperature and the AH are correlated with a coefficient of correlation of 0.6. Given the location-specific temperature and the AH of the incoming air, the RH at any point on the surface of the canister can be calculated.

The model is currently being updated, and the time step has been decreased to ½ day to capture diurnal variations in ambient weather. Also, 64 different weather data sets, representing weather stations as close as possible to existing ISFSIs, have been implemented. This will allow future versions of the model to assess the effect of geographical variations in weather (ambient temperatures and AH) on predicted SCC initiation and growth rates.

Limiting RH for Corrosion

Since the composition of the deposited salts is assumed to be sea-salt, the deliquescence properties are also assumed to be those of sea-salts. As discussed in Section 2.5.4, there is considerable variability in proposed threshold RH values for corrosion, and it may vary with the deposited salt load. For the SNL model, a value of 15% RH was conservatively chosen. A sensitivity analysis was performed using a threshold value of 20% to assess the importance of this parameter.

3.1.3.2 Tensile Stress Model

In the SNL SCC model, it was assumed that only residual stresses related to welding are sufficient to promote SCC. There are no direct measurements of residual stresses associated with typical UNF dry storage casks welds, although Sandia National Laboratories is currently assessing the residual stresses in a full-diameter cylindrical canister mockup. The through-wall stress profiles used current SNL SCC model are from weld residual stress modeling performed by the NRC (Kusnick et al. 2013). The stress profiles were calculated for longitudinal canister welds, and are those for tensile stresses parallel to each weld, which are largest and which are tensile, and in fact, greater than the uniaxial yield stress, throughout the wall thickness. The NRC (Kusnick et al. 2013) evaluated both isotropic and kinematic hardening laws, and noted that the real stresses would lie between the two model profiles. For the probabilistic model

described here, the kinematic and isotropic model curves for the longitudinal welds were discretized, and a stress curve was generated by linearly interpolating a randomly generated position between the curves for the two models. For each realization, a value x between 0 and 1 was sampled, the isotropic curve was multiplied by x and the kinematic curve by (1-x), and the results are added together. The summed curve was used in that realization. As a sensitivity analysis, a case was run assuming a constant tensile stress equal to the yield stress of the metal, assumed to be 215 MPa (note that stresses predicted by the NRC were generally much greater than that).

3.1.3.3 Pit Initiation Model

In the initial version of the SNL model, a statistical approach was used for modeling the formation of stable pits. However, due to lack of relevant data, conservative parameters were chosen to result in instant stable pit formation once deliquescent brine formed. This model is currently undergoing a major revision using the equations from Engelhardt and Macdonald (1998). However, the results are expected to be the similar. Because deliquescent brines are highly concentrated and very corrosive, stable pits are anticipated to form quickly relative to storage time intervals, once the canister location has cooled enough so that the surface RH $\geq$ RH_L. Implementation of a model that limits pit growth as a function of chloride surface load (e.g., Chen and Kelly, 2010) might result in more significant incubation times, and is also being considered.

3.1.3.4 Pit Growth Model

The pitting growth model that is used is that described in Turnbull et al. (2006a). It has the form:

$$x_{pit} = \alpha_{pit} t^{\beta_{pit}} \qquad \text{Eq. 3-7}$$

where x_{pit} is stable pit depth, t is time after initiation, α_{pit} is a scaling factor, and the exponent β_{pit} is, in part, a function of the pit geometry and determines the shape of the growth curve with time. Parameters α_{pit} and β_{pit} are generally determined experimentally for a given system. However, given the lack of relevant experimental data, a different approach was used. Some theoretical constraints can be placed on β_{pit}, which is a function of the pit geometry. For a fixed corrosion rate and a hemispherical pit, β_{pit} is equal to $^1/_3$ (Kondo 1989). Zhang et al. (2013) summarizes values for β that have been observed experimentally for many different systems and alloys, and several researchers have observed pit growth rates that are a function of $t^{1/3}$. Growth rate exponents as large as 0.596 have been reported, but the most commonly observed rate relationship is the pit depth increasing as a function of the square root of time (β = ½). This may represent a condition where pit geometry is not the dominant factor in controlling penetration, but rather the corrosion rate is becoming limited by diffusion of reactants into and out of the pit (e.g., Scheiner and Hellmich, 2007). A likely range of values for β, therefore, is 0.3 to 0.5 (Zhang et al. 2013), and for the SNL model, β_{pit} is uniformly sampled over that range.

Then α_{pit} is determined. This parameter is strongly controlled by the environment of corrosion, and relevant data are not available. To estimate α_{pit}, the SNL model makes use of the experimental observation that pits transition to stress corrosion cracks at depths of 50-70 μm. This transition occurs, according to the pit-to-crack transition model implemented here, when the pit growth rate, which decreases with depth, is equal to the calculated crack growth rate, which increases with depth (Kondo 1989). Therefore, for each realization, the pit growth parameter β_{pit} is randomly selected from 0.3–0.5, and the pit growth parameter α_{pit} is chosen such that the pit growth rate is equal to the calculated crack growth rate for that realization and time step (Section 3.1.3.5), at a randomly selected depth of 50-70 um.

3.1.3.5 Model for Conversion of Pit to SCC Crack.

As a corrosion pit grows, it acts as a stress focuser, and should SCCs form, they are commonly observed to originate from corrosion pits (Kondo 1989; Turnbull and Zhou, 2004; Turnbull et al. 2006a, 2006b; Nakayama 2006; Kosaki 2008; Prosek et al. 2009; Albores-Silva et al. 2011; Shirai et al. 2011a). The depth at which the transition from pit to crack occurs is generally based on one of two criteria (Zhang et al. 2013):

- the calculated stress corrosion crack growth rate, which increases with depth because it is a function of the crack tip stress intensity factor, exceeds the corrosion pit growth rate, which decreases with depth (Kondo 1989);
- the pit depth increases to the point that the equivalent surface crack would have a stress intensity factor (K) that exceeds the threshold stress intensity factor (K_{th}) for SCC growth.

The model implemented is that described in Turnbull et al. (2006a, b) and uses the Kondo (1989) criterion. To do this, both growth rates are calculated each time step, and the pit is assumed to transition to the crack when the crack rate exceeds the pit rate. It should be noted that this model is a simplification; recent studies have shown that cracks sometimes initiate on pit sides rather than pit bottoms, due to localized stress concentrations (Turnbull et al. 2009; Turnbull 2014; Zhang et al. 2013).

3.1.3.6 Crack Growth Model

SCC crack growth rates are a function of many different factors and can be expressed in the following general form (for example, Wu and Modarres, 2012; EPRI, 2014c):

$$dx_{crack}/dt = \dot{x}_{crack} = \alpha_{crack} \cdot f(T) \cdot f(K) \cdot f(R_a) \cdot f([Cl^-]) \cdot f(pH) \cdot f(\sigma_{ys}) \ldots \quad \text{Eq. 3-8}$$

Where α_{crack} is the crack growth amplitude factor (or, the crack growth rate at a fixed reference set of conditions), and that value can be modified by many other factors, including material property factors such as the stress intensity factor (K), degree of sensitization (R_a), and yield stress (σ_{ys}); and environmental factors such as temperature (T), chloride concentration ([Cl^-]), the mass of chloride per unit surface area (m_{Cl}), and the solution pH.

The effects of K and T are included in the SNL model; the other factors are not considered explicitly, but are included implicitly in the experimental data sets used to parameterize the SCC growth rate. The experimental data sets include base metal, weld, HAZ, and sensitized samples, and both 304 SS and 304L SS, capturing the effects of different R_a and σ_{ys} values. Similarly, the experimental data are based on samples exposed to sea-salts and sea-spray at different RH conditions, matching the conditions of interest; therefore [Cl^-] and solution pH are implicitly included in the model.

For a model accounting for K and T, a power law dependence is assumed for K, while an Arrhenius relationship is assumed for the temperature dependence (Wu and Modarres 2012):

$$\frac{dx_{crack}}{dt} = \alpha_{crack} \cdot exp\left[-\frac{Q}{R}\left(\frac{1}{T} - \frac{1}{T_{ref}}\right)\right] \cdot (K - K_{th})^{\beta_{crack}} \quad \text{Eq. 3-9}$$

where:

dx_{crack}/dt is the crack growth rate

α_{crack} is the crack growth amplitude

Q is the activation energy for crack growth [kJ/mol)]

R is the universal gas constant (8.314 J mol^{-1} K^{-1})

T is the temperature (K) of interest

T_{ref} is a reference temperature (K) at which α was derived. To be consistent with the PNNL thermal model, a reference temperature of [288.71K] 15.55ºC (60ºF) is used as the reference temperature.

K is the crack tip stress intensity factor [MPa√m]

K_{th} is the threshold stress for SCC

β_{crack} is the stress intensity factor exponent.

…

The stress intensity factor K is defined as (Wu and Modarres, 2012):

$$K = \sigma_{applied} Y \sqrt{\pi x_{crack}} \qquad \text{Eq. 3-10}$$

where $\sigma_{applied}$ is the tensile stress determined from the weld residual stress model (Section 3.1.3.2), Y is a shape parameter, equal to 1 for an infinite flat plate, and x_{crack} is the crack depth.

Parameterization of the Crack Growth Model

***Threshold Stress Intensity*—**The threshold stress intensity factor for SCC, K_{th}, was estimated to be 1.97 MPa√m. This was determined by using the stress profile calculated for the kinematic hardening law (Section 3.1.3.2) which is the lowest possible stress profile for the model. The K value was then calculated for a depth of 25 µm, assumed to be the minimum depth possible for a stable pit.

Stress Intensity Factor Exponent—Based on literature values, the stress intensity factor exponent, β_{crack}, was sampled from a normal distribution with a mean of 0.5 and a standard deviation of 0.2; the distribution was truncated at values of 0 and 1. These values were chosen to match trends in crack growth rate with K that are commonly observed. A typical example for sensitized 304 SS is given by Khatak et al. (1996) for immersion in a solution of 5 M NaCl + 0.15 M Na_2SO_4 + 3 mL/L HCl at 108ºC. Once a threshold of about 10 MPa√m is exceeded, the crack growth rate increases rapidly with increasing K, but reaches a plateau value at a K of about 15 MPa√m, and does not change with further increases in K. The plateau is generally attributed to crack growth becoming transport limited. The chosen values for β_{crack} yield a very similar pattern, as is shown in Figure 3-3. The SNL model crack growth rates are slightly non-conservative, increasing somewhat more slowly with increasing K than the measured rates. However, the general relationship is well captured.

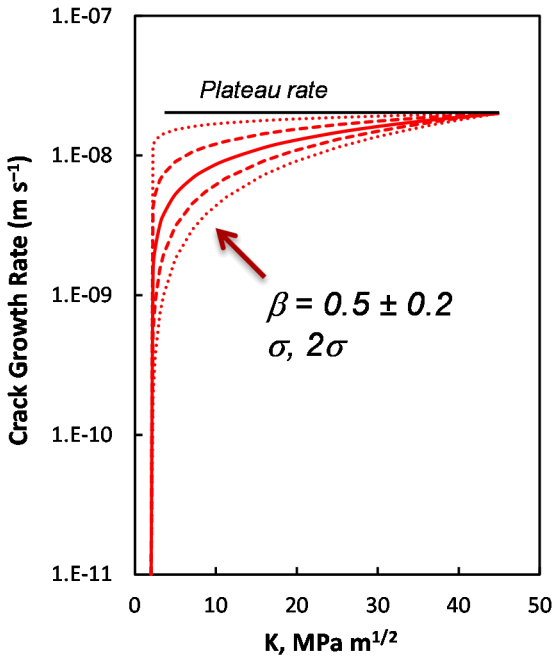

Figure 3-3. Crack growth rates as a function of K, calculated by the SNL probabilistic SCC model.

Derivation of Q and α_{crack}—The data from which Q and α_{crack} were derived are shown in Figure 3-4a. Data used in the model was restricted to that representing atmospheric corrosion of SS due to deliquescence of marine salts, or marine salt components, on the metal surface. A suite of experimental studies, representing both long-term field tests and accelerated laboratory tests, has been identified. All of these data were collected specifically to address the issue of UNF dry storage canister corrosion. Data are limited to rates from 304 SS, and they include base metal, weld, and sensitized samples (Hayashibara et al. 2008, Kosaki 2008, Tani et al. 2009, Cook et al. 2011, Shirai et al. 2011[a], Nakayama and Sakakibara 2013). There is a good deal of scatter in the measured rates, however, the rates do suggest that if deliquescence and corrosion can initiate at temperatures of 50º to 60ºC, then canister penetration could occur within anticipated storage intervals. It should be noted that the long-term crack growth data collected by CRIEPI (Section 3.1.1.4), which indicates much slower crack growth rates as the crack deepens, were not included in the growth rate data used for the SNL model As described in Section 3.2.2.1, experimental methods (use of a bend specimen with depth-varying stress conditions; salt deposition as a small droplet) may have resulted in artifacts in the measured rates. The CRIEPI data, if verified, greatly reduce the estimated risk of canister penetration by SCC, and confirmation of these data is a research priority.

Model Implementation

Crack growth rate parameters in the SNL model are sampled once per realization First, the value of β_{crack} is sampled from a normal distribution ($\mu = 0.5, \sigma = 0.2,\ min = 0,\ max = 1$) that captures observed literature values for that parameter. Then, crack growth rates and activation energies are sampled from the literature data set, with uncertainty. The crack growth rates are sampled by assuming a linear fit between (natural) log of crack growth and inverse temperature (in Kelvin) (Figure 3-4a), and calculating a standard deviation around that line. The best-fit line, and two standard deviations above and below it are shown in Figure 3-4b. A crack growth rate is sampled from the distribution once per realization for the reference temperature (15.5ºC, the reference temperature for the canister thermal model), and the crack growth rate equation is inverted to estimate α_{crack} and the activation energy (E_a). Once α_{crack}, β_{crack}, and E_a

have been determined, the crack growth rate as a function of T and K can be estimated as a SCC crack progresses through the canister wall at any given location on the canister surface. Estimated crack growth rates (n = 5000) are also shown in Figure 3-4b, illustrating that the method accurately captures the uncertainty in the measured crack growth rate data.

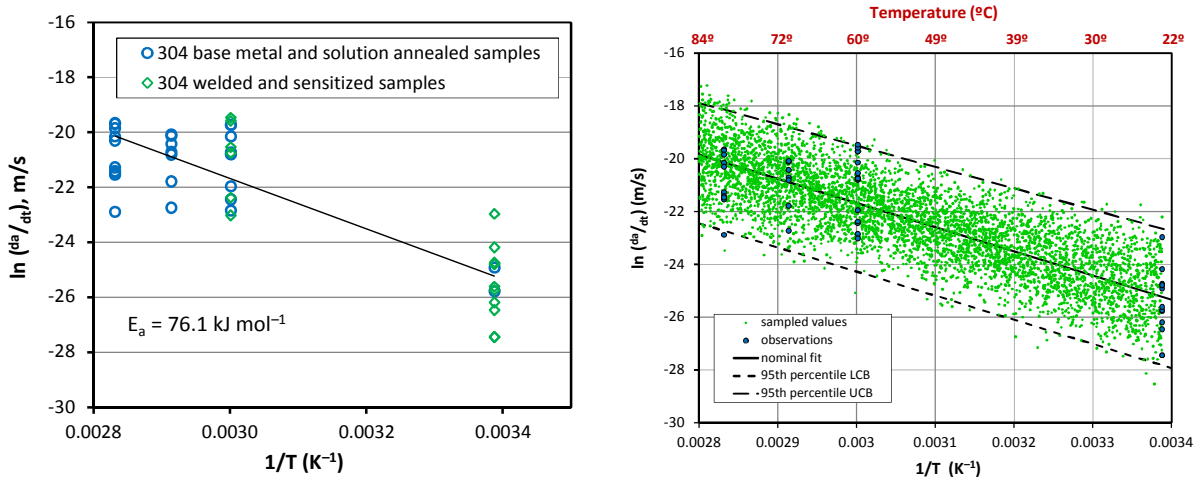

Figure 3-4. a) Measured crack growth rate data used to parameterize the CGR model in the SNL probabilistic model, b) Result of Monte Carlo estimation of uncertainty over Crack Growth Rate

3.1.4 Summary

All the models considered canister surface temperatures and relative humidity and modeled that there would be no initiation or growth of cracks when the calculated surface RH was below either the DRH or RH_L. All the models conservatively assumed sea-salt as the only deposit on the canisters. Some aspects of SCC initiation were considered by some models including: chloride accumulation, the threshold chloride surface density (CSDT) for SCC, and the mechanism for SCC initiation. The CGR is influenced by many factors including crack depth, temperature, stress intensity factor, sensitization, surface chloride concentration, surface finish, iron contamination, alloy, and others. However, due to lack of data, only three terms were explicitly included in the CGR models, a base rate at reference conditions (α_{crack}), a temperature term, and a stress intensity term.

$$CGR = \alpha_{crack} \cdot f(T) \cdot f(K_I) \quad \text{for RH} \geq \text{DRH or } RH_L. \qquad \text{Eq. 3-11}$$

These are summarized in Table 3-2.

Table 3-2. Comparison of Models

Model or Parameter	**CRIEPI**	**EPRI**	**SNL**
Model Type	A collection of submodels including conservative single values and empirical fits to data	Deterministic model using real hourly weather data and assumed canister surface temperature offsets.	Example probabilistic model using abstracted real daily weather and calculated canister surface temperature distributions
Surface Temper-ature	Linear fit versus time for one location independent of ambient T.	Assumed initial temperature offsets from ambient with decay. One year of hourly ambient data from 7 locations	Interpolation between 35 grid points as a function of decay heat and ambient temperature. Daily ambient data with uncertainty from one year of data from an example site
Surface RH	Calculated at least daily at one surface location	Calculated hourly for T_{offset} ranging from 0 to 35C.	Calculated daily for many surface locations of an example horizontal canister at several initial canister power levels. Ambient temperature and AH are correlated with a coefficient of correlation of 0.6.
DRH or RH_L	RH_L = 15%	DRH = DRH_{MgCl2} – 7% offset (about 20 to 25% in temperature range of interest)	RH_L = 15%
Chloride Density	Empirical model	Assumed sufficient for SCC	Assumed sufficient for SCC
CSDT	from 0.3 g/m^2 to 2.3 g/m^2	Not applicable	Not applicable
SCC initiation	Occurs when CSD ≥ CSDT	Not applicable	Pit initiation, growth, and transition to SCC models
CGR coefficient α_{crack}	Fast growth to 2mm, CGR = 1e-11 m/s there after	Conservative statistical treatment on a limited data set. 168 mm/yr (5e-9 m/s) for crack depth < 3.16 mm, 2.2 mm/yr (7e-11 m/s) for crack depth ≥ 3.16 mm	sampled from all available data
CGR Tempera-ture term $f(T)$	Single conservative temperature (80ºC) used ($f(T)$=1)	$f(T) = exp\left[-\frac{E_a}{R}\left(\frac{1}{T(t)}-\frac{1}{T_{ref}}\right)\right]$ T_{ref} = 80ºC E_a = 40 kJ/mol	$f(T) = exp\left[-\frac{E_a}{R}\left(\frac{1}{T(t)}-\frac{1}{T_{ref}}\right)\right]$ T_{ref} = 15.55ºC E_a sampled from data
CGR Stress intensity term $f(K_I)$	Discussed but not included	$f(K_I)$ =1 when K_I >0, $f(K_I)$ =0 when $K_I \leq 0$	$f(K_I) = (K_I - K_{th})^{\beta_{crack}}$ $K_I = \sigma_{applied} Y \sqrt{\pi x_{crack}}$ K_{th} = 1.97 MPa√m β_{crack} = normal dist. ($\mu = 0.5, \sigma = 0.2, min = 0, max = 1$)

3.2 Model Limitations

3.2.1 CREIPI

3.2.1.1 Surface Temperature

Shirai et al. (2011a) included a function for the evolution of temperature at the bottom of the canister over time since emplacement. This function predicts high temperatures, and the RH_L is not reached for over 40 years. In addition, there is no allowance for the change in surface temperature with ambient temperature. This function is not applicable to any DCSS in the US.

3.2.1.2 DRH or RH_L

The RH_L of 15% may be realistic or conservative. Based on the work of Schindelholz et al. (e.g. Schindelholz and Kelly 2012, Schindelholz et al. 2014a) it is not clear that a time of wetness model based on a strict RH_L is correct or may under predict the timing of corrosion.

3.2.1.3 Chloride Density

The chloride deposition model described by Shirai et al. (2011a) is an empirical model for deposition on heated vertical surfaces. This model would not be applicable to any DCSS in the US, and from the data presented, it is not even clear it is applicable in Japan.

3.2.1.4 CSDT

The CSDTs for SCC obtained for the most relevant conditions are 0.3 g/m^2 of Cl from sea-salt for 50ºC 35% RH and 0.5 g/m^2 for 60ºC 25% RH. These are higher than the values of 0.02 and 0.1 g/m^2 Cl from $MgCl_2$ at which Fairweather et al. (2008) observed SCC at 60ºC; however, because sea-salts precipitate almost all NaCl at these RHs, the CSD in solution and brine thickness are actually lower than that seen by Fairweather et al. (2008). These CSDTs may be reasonable for sea-salt, but further work is needed to confirm this.

3.2.1.5 SCC Initiation

SCC is assumed to occur as soon as the CSD ≥ CSDT, and the RH threshold is exceeded. This is conservative, because there is usually an incubation period for localized corrosion to initiate and for that to progress to SCC.

3.2.1.6 CGR Parameter α_{crack}, functional dependence on T and K_I

The CGR is not given as a function of temperature or K, but a single rate obtained under limiting conditions is used. The recommended CGR of 1e-11 m/s is based on a series of 4-point bend tests. Four tests were run, three with synthetic sea-water, and one with saturated $MgCl_2$ solution. The experimental setup was as follows: the sample is 10 mm x 20 mm x 220 mm, the conditions are 270 MPa surface stress, 80ºC, 35% RH, and about 10 g/m^2 chloride from artificial sea water. The CGR was calculated from reverse current potential drop method data assuming propagation of a half elliptical crack with a constant aspect ratio determined by post-test examination of the sample. The sea water tests showed an initial rapid CGR followed by a much slower CGR of about 1e-11 m/s, while the $MgCl_2$ test showed only a fast rate. Results of one sea water test are shown in Shirai et al. (2011a, Figure 11), and Shirai et al. (2012), but the data for all four tests are only provided in the CRIEPI report describing the experiments (Shirai et al. 2011b, Figure 3-6). Shirai et al. (2012) indicate that the solution was applied as a spray using the Methods of Salt Spray Testing (JIS Z 2371). However, Shirai et al. (2011b) describe the application of

the test solution as a 20µl drop in the center of the sample and provide an illustration of the deposition method, contradicting the description in Shirai et al. (2012).

The CRIEPI report also describes the crack geometry as half elliptical with a/c ranging from 0.5 to 1 (where "a" is the crack depth and "c" is ½ the crack surface length). After they performed calibration experiments on the potential drop method, they state:

> "*This suggests that the potential difference is dependent on simply the cross-sectional area alone, regardless of the shape of the crack.*"

The reported crack depths were calculated assuming a constant crack aspect ratio, although the ratio was not specified for each test. This assumption is most likely incorrect. Newman and Raju (1981) have shown that for fatigue crack growth under bending, no matter the starting a/c, the a/c will quickly follow the line where a/c = 1 – (a/t). This is because of variations in *K* along the perimeter of the crack, and the dependence of the CGR on *K*. It is not clear that this relationship is applicable to SCC, which also faces constraints related to reactant transport, but if it is applicable to these bending tests, the a/c would start at 1 and decrease to 0.6 at 4 mm depth. Hence, calculated crack depths, which assume a constant aspect ratio, would be incorrect.

Table 3-3 provides the CGR calculated by Shirai et al. (2011b) based on the assumption of constant a/c. Table 3-3 also shows information obtained by estimation from the figures provided in Shirai et al. (2011b). The data show strong trends that allow for good fits, but also show significant scatter around those trends. This can be seen in Column 5 where the ranges in crack depths seen at the end of the experiments are provided.

Table 3-3. CRIEPI 4-Point Bend Test Results

Test	Slow Rate Fit (m/s)	Transition Depth (mm)	Fast Rate Fit (m/s)	Crack Depth at End of Test (mm)	Test Duration (years)
Sea-salt 1	1.60e-11	2.7	4.40e-10	2 to 3.3	0.42
Sea-salt 2	7.60e-12	2.0	2.20e-10	1.7 to 2.5	0.91
Sea-salt 3	2.20e-12	1.7	1.70e-09	1.5 to 1.75	0.91
	Rate 0 to 2 mm depth	**Rate 2 to 3.5 mm depth**	**Rate 3.5 to 4 mm depth**		
$MgCl_2$	5.60E-10	2.40E-10	1.10E-10	3.6 to 4	0.42

Shirai et al. (2011a) and (2012) do not attempt to explain the bimodal behavior seen with sea-salt but not with $MgCl_2$. Shirai et al. (2011b) suggested that the slowing of the crack growth rate might be in part at least, due to the decrease in stress at the crack tip in a bending specimen as the crack propagates deeper into the sample.

> "*In all case where the artificial seawater was applied, the cracks in the test samples grew to a depth of approximately 3 mm at a relatively fast rate of crack growth when in a state where the bending tensile stress at the surface, immediately after the start of the test, was predominant. Then there was a tendency for the speed to drop according to the redistribution of the stress. On the other hand, with the test pieces to which the magnesium chloride was applied, the speed of growth was essentially consistent throughout the entire testing period. The initial speed of growth of the crack in the test pieces to which the artificial sea-salt was applied was essentially the same as the speed of crack growth in the test pieces to which the magnesium chloride was applied.*"

Thus, the bimodal CGR behavior of these three bending tests is not yet explained by the authors. Until the cause of this phenomenon is established, it will not be clear if these 4 point bend tests are relevant to UNF canisters, whose residual stress profiles due to welding are significantly different than the stress profiles of 4-point bend tests. Even though the 1e-11 m/s second phase CGR was obtained under unrealistically aggressive conditions, it falls significantly below the shallow CGRs found in these tests and in the literature as shown in Figure 3-3. These tests are further discussed in Section 3.2.2.5.

3.2.2 EPRI

3.2.2.1 Surface Temperature

As described above, EPRI does not try to model the temperature distribution across the canister but instead calculates the CGR for T_{offset} (the difference between the ambient and canister surface temperatures) ranging from 0 to 35ºC. For sensitivity calculations, the time for through wall crack growth was determined with the initial T_{offset} set at 35ºC, 25ºC, and 15ºC. The T_{offset} is assumed to be proportional to the power that is decayed using a generic power decay curve. To apply the EPRI equations to a particular canister, the distributions of T_{offset} across the canister, through time, must be calculated.

3.2.2.2 DRH or RH_L

The RH_L used by EPRI is the DRH model for $MgCl_2$ minus an offset of 7%. This seems a reasonable approach, but does not capture observed SCC initiation at 15% RH by Fairweather et al. (2008) and Shirai et al. (2011a). As mentioned in Section 2.5.4, values as low as 11% may apply for mild steel at sufficiently high salt loadings. It is not clear if this would be true for 304 SS.

3.2.2.3 Chloride Density Modelling and CSDT

Not Included.

3.2.2.4 SCC Initiation

Not Included.

3.2.2.5 CGR Parameters α_{crack}, functional dependence on T and K_I

CGR dependence on Stress Intensity Term (K_I)

As mentioned in Table 3-2, EPRI conservatively assumed that $(K_I) = 1$ when $K_I > 0$, and $(K_I) = 0$ when $K_I \leq 0$. As discussed in their Section A.2.2.1, this was based primarily on data by Kosaki (2008), which showed CGR independent of K_I between 0.5 and 30 MPa$\sqrt{m}$. This behavior is not the typical behavior in immersed conditions, as described by Jones (2003). Data for sensitized 304 SS in acidified boiling NaCl solutions shown by Khatak et al. (1996) is very similar to that of solution annealed 304L SS in a solution of 42% $MgCl_2$ at 130ºC shown by Spiedel (1997, Figure 2). These show a threshold stress intensity factor (K_{ISCC}) of about 8 MPa$\sqrt{m}$, a rapid rise in CGR with K, and a plateau with a CGR of about 2×10^{-8} m/s which is reached before about 15 MPa$\sqrt{m}$. Spiedel's Figure 6 shows data curves for austenitic steels for a wide range of immersed conditions. They all show a similar K_{ISCC} and a transition to a plateau around 15 MPa$\sqrt{m}$, but the CGR at the plateau is different for each. As explained by Jones (2003) the K_{ISCC} and the plateau are the result of synergistic interaction between the metal with the environment, and both vary with environmental parameters. The CGR at the plateau determined by the rate-limiting processes effective in that K range, such as mass transport of species to the crack tip. Because the cathode and chemical conditions in immersed conditions are so different from that under atmospheric conditions, the CGR – K_I dependence may be significantly different, and the Kosaki data suggests this is the case.

However, it is difficult to assess the Kosaki data due to the limited information provided about how the tests were run. These tests were performed using welded and unwelded samples of 304 SS, 304L SS, and 316LN SS under natural conditions at the Miyakojima island site and under accelerated conditions which were described as

> *"Test temperature: 60ºC, humidity: 95% RHS, environment filled with NaCl steam mist (at the surface of the test specimen is the saturated NaCl concentration)."* The tests were run *"using small 3-point bending test specimens…. The test piece is 10 mm in thickness x 15 mm in width x 90 mm in length with two types of pre-cracks induced by fatigue (through crack and half-elliptical surface crack). These were loaded with 0.4 PS or 0.8 PS. After the corrosion tests, the loading stress onto the test specimens was measured and the loading tools removed. After including post-crack by fatigue the section of test specimens were fractured and the maximum depth of SCC cracking measured by an optical microscope and an electron microscope."*

For the welded samples, the middle pressure point of the tool was positioned over the HAZ (Kosaki 2008, Figure 5). The results are provided in plots of da/dt versus K_I, with K_I ranging from 0.5 to 30 MPa√m. For both the natural and accelerated conditions, the points for all 6 specimen types form a scatter about 1.5 orders of magnitude wide that is independent of K_I. From the information provided, it seems that the calculated d*a*/d*t* data includes crack growth in all directions from vertical to the crack tip to horizontal along the surface. Assuming a yield strength of 300 MPa, some simple calculations using the test geometry and the equations of Newman and Raju (1979) for pure bending show that to obtain a K_I as low as 0.5 MPa√m, the crack depth must be less than about 10 μm; it is also difficult to obtain a K_I as high as 30 MPa√m. Because the method of determining the location-specific stresses and K_Is are not provided, it is impossible to assess the validity of the K_Is used in the plots.

CGR Parameters α_{crack} and Transition Depth

There is only one study that measures CGR as a function of depth on thick samples - Shirai et al. (2011b). The sea-salt samples show two phases of crack growth – a fast shallow phase with CGRs consistent with other shallow CGRs in the literature, and a slower deep phase with much slower CGRs. Based on this study, EPRI developed two α_{crack} values, and a transition depth. This study is also one of the two that met EPRI's criteria for inclusion in the parametrization for the α_{cracks}. EPRI excluded the other data for several reasons. Data obtained on specimens that were exposed to solar heating were excluded because of the resulting uncertainty in surface temperature. Only data using sea-salt and only data where initiation time could be excluded were used (experiments using a sharpened pre-crack or continuous measurement).

The experiments of Shirai et al. 2011b are discussed here as they are the basis for the EPRI Model. These are the tests already introduced in Section 3.2.1.6.

Crack tip stress intensity Factor (K_I)

EPRI calculated the K_I values for these 4-point bend tests using the equations of Newman and Raju (1979) and concluded that the changes in K_I with depth were not responsible for the observed behavior. These calculations are repeated here for the end member a/c values of 1 and 0.5. The curves for a crack across the full width of the sample and that for a crack within an infinite plane are also shown for comparison. The geometry of the cracked sample is shown in Figure 3-5. Figure 3-6 shows the calculated K_I with depth for various configurations. The dotted portion of the lines show where the equations are exercised outside their valid range. Figure 3-7 shows a close-up of calculated K_I in the range applicable to the test with a range of a/c values consistent with the test. The transition depths for the three tests are also shown.

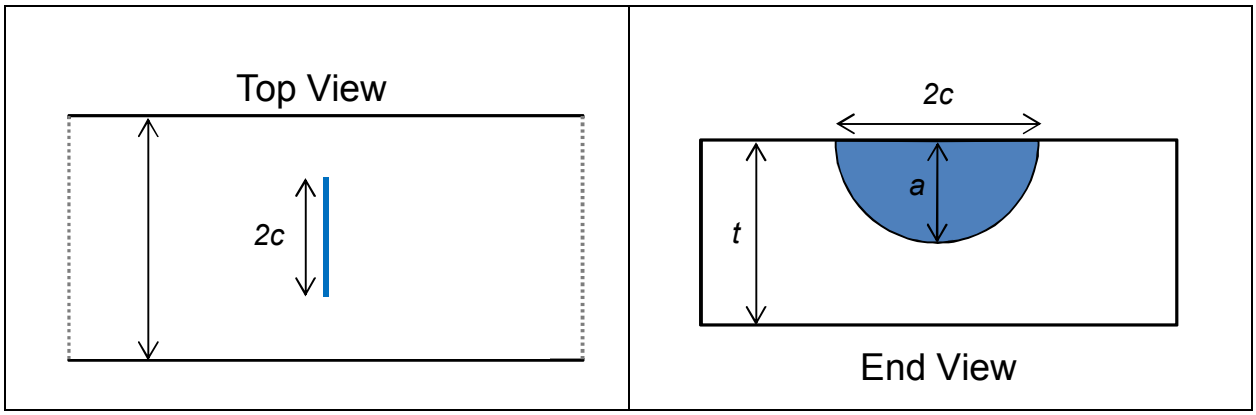

Figure 3-5. Sample and crack geometry.

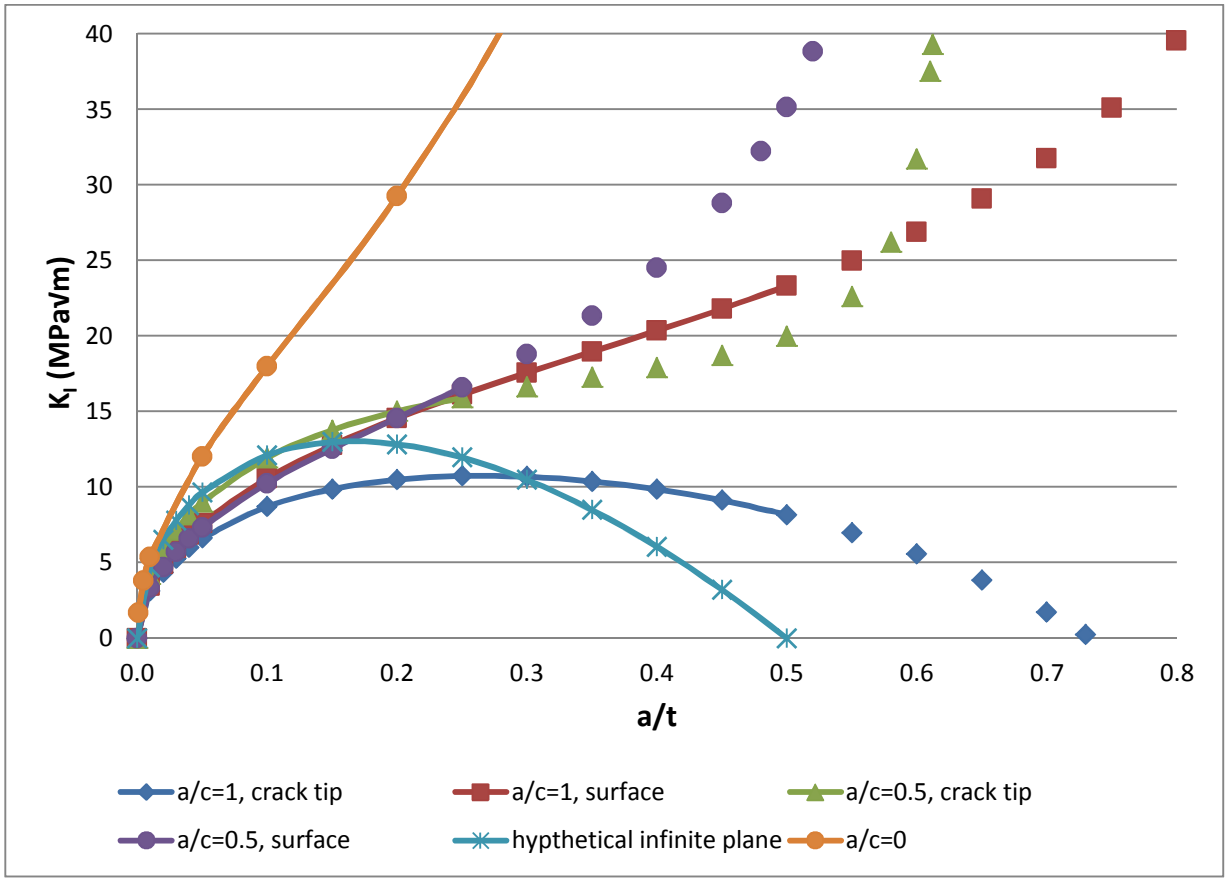

Figure 3-6. K_I as a function of location along the crack (bottom "tip" or surface), for different crack aspect ratios.

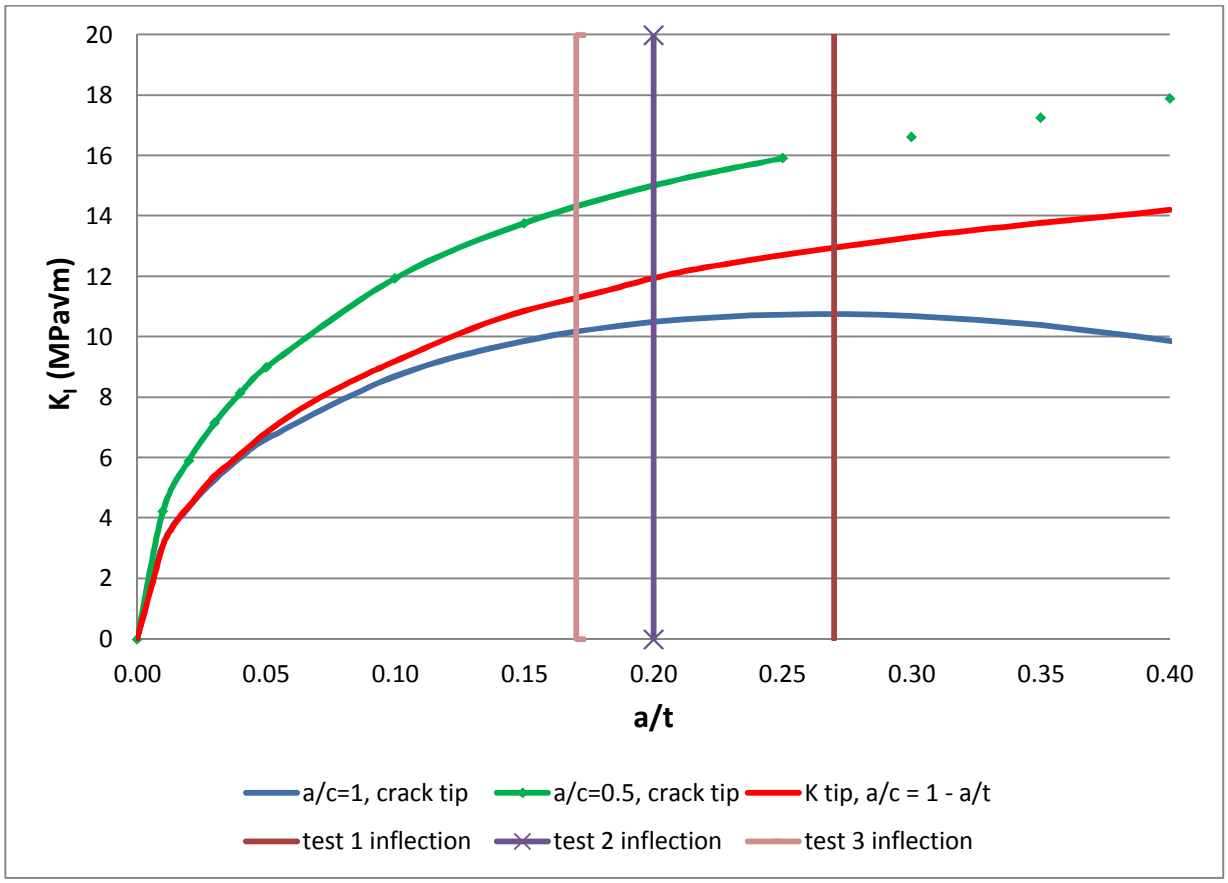

Figure 3-7. K_I as a function of aspect ratio, at the bottom of the crack, compared to inflection points in Shirai et al. (2011b) CGR data sets.

EPRI's assessment that the K_I values do not account for the observed behavior is probably correct. If typical CGR- K_I behavior was seen, the CGRs would increase rapidly to some plateau and remain very high, thus the slope of the curves would increase to a fixed large value. The opposite is seen in the CRIEPI experiments; the CGR starts at a high fixed value and then drops to a lower fixed value. However, the results are also inconsistent with an increasing degree of cathodic limitation as the crack grows deeper, as this would be exhibited as a continued slowing in crack growth rate.

Mechanism

EPRI suggests the

> "*mechanism for a reduction in propagation rate with depth is a limiting of the corrosion current that can be supplied by the cathodic area on the material surface as the crack tip—the anode—moves further away, thereby increasing the ohmic resistance. For immersed specimens, the aqueous cathode area is very large, which generally prevents such a limiting effect. The presence of particulates in the electrolyte layer significantly reduces the cathode capacity (1) through increased ohmic resistance, (2) by interrupting the cathode continuity, and (3) by impeding the transport of oxygen [Kelly et al. 2006]. The partially deliquesced state of sea-salt over the most relevant range of RH [He et al. 2014a] results in the observed crack stifling behavior. CRIEPI experiments using pure $MgCl_2$, which fully deliquesces at 35% RH, did not exhibit the same effect [Shirai et al. 2011b].*"

If the cathode limitation is indeed the rate reducing factor for the sea-salt tests, the CGR should decrease with depth, not stay steady.

There is some ambiguity in the dimensions of the cathode in these tests. Shirai et al. (2011b) describe the application of the test solution as a 20 µl drop in the center of the sample and also claim a 10 g Cl/m^2 chloride surface density. Thus two cases were evaluated here, first assuming the brine formed a hemispherical drop and second, assuming the brine spread to achieve a surface load of 10 g/m^2. Results are shown in Table 3-4.

Table 3-4. Possible surface drop dimensions for the CRIEPI 4-point bend tests

	Surface dimensions (mm)	**Brine thickness (µm)**	**[Cl] Molar**	**CSD (g/m^2)**
Sea-salt hemisphere drop	4.2 diameter	6.92 obstructed by precipitated NaCl	10.4	28
$MgCl_2$ hemisphere drop	4.2 diameter	1400	11.6	582
Sea-salt spread to 10 g/m^2	7.1 diameter	2.47 obstructed by precipitated NaCl	10.3	10
$MgCl_2$ spread to 10 g/m^2	20 x 41	24	11.5	10

As can be seen in Table 3-4, the possible cathode dimensions are significantly different for sea water, which concentrates and precipitates NaCl under the test conditions, versus saturated $MgCl_2$ which does not. For hemispherical drops, the brine thicknesses are more than 2 orders of magnitude different. For drops spread out to 10 gCl/m^2, both the area and brine thickness are much larger for the $MgCl_2$ test. Thus cathode limitation is much more likely for SCC under sea salt than under a similar load of $MgCl_2$. However cathode limitation alone would result in a continually decreasing CGR, not 2-phases of CGR. Other changes in rate determining steps are likely occurring and are yet unexplained, thus calling into question the usefulness of this data in the development of an SCC predictive model. ***CGR Parameters***

Due to the small sample sizes, a statistical treatment was used to provide conservative values for the α_{crack} values and the transition depth as follows.

> "*The log-normal distribution is used for the two CGR coefficients while the normal distribution is applied to the transition depth. For each of the three parameters, the best-fit plots and the fit using the upper bound of the 50 percent confidence interval (75th percentile) mean with a fitted standard deviation are plotted against the data in Figure A-6, Figure A-7, and Figure A-8. For the CGR calculations performed in this report, the 95th percentile value of this conservatively fit distribution is used.*"

It is not clear that this statistical approach compensates well for the lack of additional data.

CGR Coefficient Shallow Growth (First Phase)

The α_{crack} for the shallow phase was developed from the two sets of experiments that met EPRI's criteria: Shirai et al. (2011b) as already discussed, and Tani et al. (2009). The Tani et al. (2009) experiments were performed on

> "*316L CT specimens at 35% RH and temperatures of 50ºC and 80ºC. A drop of seawater was placed inside the machined notch and various K_I values from 5 to 30 MPa(m)$^{0.5}$ were applied. Both of these tests used potential drop measurement techniques to continually monitor crack depth. All the sea-salt*

tests in Reference [Shirai et al 2011b] *exhibited bilinear growth with an initial growth rate before about 2 mm of depth followed by a slower steady state growth rate; only the shallow CGRs are used for the first phase growth coefficient.* [Tani et al. 2009] *contained data at 50ºC that were consistent with an activation energy of 190 kJ/mol. These were conservatively omitted because they would significantly reduce the mean value.*"

The chosen CGR were compared to two sets of shallow CGR determinations that did not meet the EPRI criteria. The data of Shoji and Ohnaka (1989), Hayashibara et al. (2008) and Kosaki 2008

"*is within the inherent scatter of (and typically slower than) the data set used to develop the CGR coefficient fit, it remains appropriate to not explicitly include initiation-plus-growth data in the statistical fit.*"

Due to the small sample size a statistical treatment was used.

CGR Coefficient Deep Growth (Second Phase)

This data is already discussed above,

CGR Transition Depth (a_{trans})

The statistical treatment led to a transition depth of 3.16 mm which bound the values shown in Table 3-3.

CGR Temperature term (T)

As shown in Figure 3-4a, there is a large spread in the data, and as discussed by EPRI, Hayashibara et al. (2008)

"*supports activation energies from 25 to 105 kJ/mol, with greatest support for the 30-40 kJ/mol range. Because the α_{crack} values were determined at a high temperature (80ºC), the use of a low activation energy (40 kJ/mol) is conservative."*

3.2.3 SNL

3.2.3.1 Surface Temperature

The thermal model within the SNL model provides temperature data for 35 grid points across the canister as a function of canister heat load and ambient temperature, but has only been constructed for a horizontal NUHOMS system. This was based on PNNL modeling of this system. PNNL has modeled, and is continuing to model, other systems, and these may be incorporated into the SNL SCC model in the future. The first iteration of the SNL SCC model exercised the thermal model using daily ambient temperatures. However the model can accommodate ambient temperatures of any frequency. In the first iteration of the SNL model, ambient data from one year at one site was abstracted into a format for probabilistic modeling. In the 2nd iteration, ambient data was collected from airports near all the existing ISFSIs in the US, and a 12 hour time step will be used.

It is not possible to thermally model all of the 40 or so different dry cask storage systems that are currently in use. The SNL SCC model is currently limited to the NUHOMS horizontal system that was thermally modeled by PNNL, and thermal histories for one typical vertical system are currently being incorporated. Therefore, extrapolation of this model to different sites, with a wide variety of canister types, will introduce potentially significant uncertainties in the results.

3.2.3.2 DRH or RH_L

Like CRIEPI, SNL used a RH_L of 15% for the base case. As discussed in Section 2.5.4 this value is likely dependent on many factors. Also the use of an RH_L to determine the time of wetness when the daily swings in RH cross this value may be incorrect, as the time for dryout may be significant. A sensitivity analysis preformed with the model identified this parameter as being very important to the predicted penetration times.

3.2.3.3 Chloride Surface Density Modelling and CSDT

The SNL does not include chloride deposition or volatilization models, but conservatively assumes that any CSDT is exceeded. In addition, the experimental CGRs used to parameterize the modeled CGRs were collected under heavy salt loading. These conservatisms may result in significant underestimation of the time for SCC to initiate and penetrate a canister.

3.2.3.4 SCC initiation

While Jones (2003) reports the possibility of SCC initiation on bare surfaces, the preponderance of evidence under atmospheric conditions is that SCC is preceded by local corrosion such as pits. There is very little data on pit initiation and growth rates under relevant conditions, so the technical basis for these models is thin.

3.2.3.5 CGR Parameters $\alpha_{crack,}(T)$, (K_I)

SNL used a larger set of data for parametrizing its SCC model, but used only the shallow, faster experimental growth rates. Thus, like the EPRI model, is not clear that the statistical approach used compensates well for the lack of additional data. The single set of deeper growth rates that are considerably slower have been excluded until the phenomenon can be verified. The probabilistic model is only as good as the input data, and thus is limited by the scarcity of data for relevant conditions.

3.3 Model Differences

Areas in which the models differ, point to unresolved issues that greatly increase the uncertainty in the predictions made by these models. The main differences are:

1. The presence or absence of deposition and volatilization models
2. A chloride density threshold for local corrosion and SCC
3. A dependence of CGR on K_I
4. A dependence of CGR on depth

Items 1 and 2 may play big roles in the predictions of SCC, however, the data and modeling needs are significant and to date have not been attempted in the US except by Calvert Cliffs in their ISFSI license renewal. However, the Calvert Cliffs models are proprietary and cannot be assessed. Chloride deposition is likely to be DCSS-design specific and will change with time as the temperatures of the canisters decrease. It may be that a sampling of the deposits on a lead canister at the time of license renewal and at some infrequent interval thereafter will provide the chloride accumulation history needed to assess the probability of localized corrosion and SCC at that site.

Item 3 hinges on limited data that suggests that the CGR may be independent of K_I under relevant conditions. This is contrary to a large amount of data under immersed conditions that indicate that at

shallow depths, CGRs should be very dependent on K_I and only when K_I is high enough should the CGR become independent of it. Since almost all data on atmospheric CISCC has been obtained on shallow samples, K_I should have some effect. A few well designed experiments may well settle this question.

More important than Item 3 is Item 4. There is only one set of data that addresses this item, and it is likely that the results cannon be generalized to different conditions. If CGR decreases with depth by 2 orders of magnitude as seen in the sea-salt samples, SCC may not be a major problem for ISFSIs. However, this phenomenon was not seen with $MgCl_2$. It is likely that at higher RH values, when the amount of brine present is larger, the CGR for sea-salts would not decrease with depth. Additional work is necessary to determine the relationship between CGR, amount of salt deposited, and RH.

3.4 Conclusions on SCC Predictive Capability

Table 3-5 summarizes the key differences and limitations for the three SSC predictive models described in Section 3. SCC cannot be defensively predicted at this time due to lack of data to resolve the issues described in Section 3.3, especially Items 2 (chloride density threshold for local corrosion and SCC) and 4 (dependence of CGR on depth). Current uncertainty in the CGRs is large, mainly due to the spread in data on shallow CGRs and sparsity of data for deep CGRs. In addition, data to support modeling of CSD and CSDT are sparse. The data collected over the next few years by the international community, by DOE, and by the nuclear industry as they perform inspections, may well settle some of these issues.

Table 3-5. Important SSC Model Differences and Limitations

Model or Parameter	CRIEPI	EPRI	SNL
DRH or RH_L model limitations	These are all based on the assumption that surface deposits will be sea salt only, and the values determined at high loads will be applicable. These assumptions are quite conservative for most if not all ISFSIs. Corrosion is assumed to occur only when the RH ≥ RH_L, which is equivalent to the assumption that the deposits will dry out as soon as the RH falls below the RH_L. It has been shown that in some cases this is not true and it may take days or longer for dryout to occur depending on the deposit composition. This assumption is non-conservative.		
DRH or RH_L differences	RH_L = 15%	Model results: ~ 20 to 25%	RH_L = 15%
CSD and CSDT	Empirical model for CSD, a CSDT of 0.3 g/m^2 to 2.3 g/m^2.	Not applicable.	Conservative assumption that CSD will be sufficient for pitting and SCC initiation.
SCC initiation	Occurs when CSD ≥ CSDT and RH ≥ RH_L	Not applicable	Pit initiation, growth, and transition to SCC models based on limited data
CGR para-	Conservative assumption that CGRs obtained under high chloride densities are applicable. Parameters for factors known to influence CGR are not included in the models due to lack of data. SNL compensates for this by using data collected under a		

meters	range of conditions that include these factors.

Table 3-5. Important SSC Model Differences and Limitations (Cont.)

Model or Parameter	CRIEPI	EPRI	SNL
CGR coefficient α_{crack}	Based on three data points obtained under overly conservative conditions. Two phases of CGR, fast CGR at shallow depths followed by slow CGR when deeper than about 2 mm.	Based on three data points obtained under overly conservative conditions. Statistical treatment used to try to compensate for small sample set. Two phases of CGR, fast CGR at shallow depths followed by slow CGR when deeper than about 3 mm.	Sampled from a large set of data for shallow CGRs obtained under both conservative and more realistic conditions. Ignores deep CGRs, and thus is has higher CGRs than CRIEPI and EPRI.
CGR Tempera-ture term $f(T)$	Single conservative temperature (80 °C) used ($f(T)$=1)	High reference temperature based on temperature from the 3 datum used and a conservatively low activation energy.	Activation energy obtained from sampled data.
CGR Stress intensity term $f(K_I)$	Discussed but not included	No dependence on K_I	$f(K_I)$ model based on sparse data
Results	SCC will not breach canister during a 60 year period	Depending on sensitivity cases, time from crack initiation to through wall penetration range from 22 to >120 years	Model not yet ready to predict penetration times, but to show which parameters most effect the calculated penetration times. Because of the exclusive use of shallow CGRs, penetration times would be short.

4. FACTORS TO CONSIDER WHEN DETERMINING AN INSPECTION FREQUENCY

The factors that could be considered when establishing an inspection frequency subsequent to the inspection of the lead cask prior to license renewal include:

1. Site and cask-specific crack initiation times and growth rate predictions,
2. Results of the inspection of the lead casks, and
3. A comparison of the risk to workers performing inspections versus risk to public of an undetected through-wall SCC.

These are discussed below.

4.1 Site and Cask-Specific Crack Initiation Times and Growth Rate Predictions

These are currently highly uncertain, but as more data becomes available and modeling techniques improve, the uncertainties may be reduced sufficiently to allow reliable predictions of SCC penetration times, or to show that penetration times will greatly exceed the license period. Specific needs include 1) site-specific atmospheric conditions (weather and aerosol compositional data); 2) data and improved modeling of chloride accumulation, SCC initiation conditions and timing, and crack growth rates; and 3) in-service inspections to provide data for model validation.

4.2 Results of the Inspection of the Lead Casks

These inspections provide site-specific data that can be used to help refine predictions of SCC both at the site and in the US overall. It is important that the results of all inspections be made available to all model developers, canister vendors, and ISFSI owners.

4.3 A Comparison of Risk

A risk comparison does not seem to have been published. EPRI's FMEA concludes that an SCC penetration is

> "*likely to be sufficiently tight to preclude the release of particulates as the inert cover gas and any accumulated fission gases escape and air enters over many weeks or years…. After a long enough cooling time, the lower temperature will reduce the rod plenum pressure and oxidation kinetics to the point where additional cladding degradation is very unlikely."*

Massari and Massoud (2011) calculated the total dose for releases through 18.4 μm holes in 72 casks loaded to design basis, using recommended release fractions and other parameters from NUREGs. The calculated doses were three orders of magnitude below the 72.104(a) limit. Therefore the dose to the public from an undetected SCC penetration is likely to be very low. However the dose to inspection workers is measurable and steps must be taken to minimize it. If a risk comparison shows that the risk to workers (once minimized by new procedures) is substantially greater than the risk to the public of an undetected through-wall SCC, minimizing the inspection frequency and number of canisters inspected may be justified.

5. OVERVIEW OF THE ONLY EXISTING AMP AND NRC'S EXAMPLE AMP

A summary and evaluation of the sections of the Calvert Cliffs DSC AMP and NUREG-1927 R1 draft for comment (NRC 2015) relevant to SCC sample frequency are provided below.

5.1 Evaluation of Calvert Cliffs Dry Storage Canister Aging Management Program

The Calvert Cliffs SCC inspection frequency is provided in their tollgate[c] in Table A1.3-1 (NRC 2014d). An initial inspection at 5 years and a subsequent inspection frequency of 10 years are based on an unpublished chloride deposition model or analysis. In the event of a detected crack, the time of completion of corrective action (5 years) is based on an unpublished crack growth rate model or analysis. NRC agreed, however, with the 5-year inspection interval as part of its approval of Exelon's Calvert Cliffs license renewal application (NRC 2014e)[d].

As concluded in Section 3.4 of this report, based on publically available data and models, SCC initiation and crack growth rates are subject to significant uncertainty. Because the Calvert Cliffs model is based on unpublished information, the technical justifications and defensibility of their parameters have not been included in this assessment and are not evaluated in this report. However, during the reassessment required at the first tollgate, this situation may be remedied.

5.2 Evaluation of NUREG-1927 Draft Revision 1

Pertinent sections of NUREG-1927 Draft Revision 1 (NRC 2015) are provided in Appendix A. An evaluation of the most relevant sections is provided in this section.

Section 3.6.1.4 "Detection of Aging Effects" provides guidance requesting inspection and monitoring details, including method or technique (e.g. visual, volumetric, surface inspection), frequency, sample size, data collection, and timing of inspections. Volumetric examination may not be field-ready for some time. The frequency must be justified, which implies some knowledge of the timing of SCC initiation and crack growth rates. As concluded in Section 3.2, publically available data and models of SCC initiation and crack growth rates are subject to significant uncertainty.

Section 3.6.1.5 "Monitoring and Trending" provides guidance requesting an evaluation of inspection results against the acceptance criteria and an evaluation regarding the rate of degradation in order to ensure that the timing of the next scheduled inspection will occur before a loss of intended function. SCC initiation and crack growth rates are uncertain and may be nonlinear based on the assessment of the publically available data and models.

The problems meeting Section 3.6.1.4 and 3.6.1.5 guidance are somewhat mitigated by the endorsement of learning AMPs in Section 3.6.1.10 "Operating Experience" as indicated by the following sentence:

---

[c] The concept of "tollgates" was introduced in NEI 14-03 to assure that future knowledge is always captured as part of operations-based aging management (NEI 2014). Periodic tollgates require reassessment of information from research and development programs, relevant domestic and international operating experience (including non-nuclear), and relevant results of domestic and international ISFSI and DCSS inspections and performance monitoring. Thus as new information becomes available and the uncertainty of SCC predictive models is reduced, a public and more defensible technical basis for inspection frequencies can be documented. See Appendix B for an example.

[d] ML14274A030.

> *"The commitment to future reviews should ensure that, as knowledge and data become available from new analyses, experiments, and operating experience, the licensees and Certificate of Compliance (CoC) holders will revise the existing AMPs (or pertinent procedures for AMP implementation) as necessary to address any deficiencies identified during the review of operating experience…"*

This section then reiterates the guidance in Sections 3.6.1.4 and 3.6.1.5, but follows with discussion of NEI 14-03 (NEI 2014) which provides a proposed framework for learning AMPs through the use of "tollgates."

The example "AMP for Localized Corrosion and Stress Corrosion Cracking of Welded Stainless Steel Dry Storage Canisters" in Table B-1 of NUREG-1927 Draft Revision 1 (NRC 2015) states:

> "*Confirmed or suspected areas of crevice corrosion, pitting corrosion and stress corrosion cracking must be assessed in accordance with acceptance standards identified in [American Society of Mechanical Engineers] ASME Section XI, IWB-3514. Flaws exceeding the acceptance standards in IWB-3514.1 must be evaluated using the acceptance criteria identified in IWB-3640."*

IWB-3514.1 specifies flaw depth in the range of 10-15% of the wall thickness while IWB-3640 outlines an assessment of crack growth rates and failure criteria but precludes cracks greater than 75% through wall during the license period.

However, this example AMP may not be readily implementable due to the uncertainty in current predictive models that may not support justifiable inspection frequencies. Areas with indications of corrosion detected during inspection are to be further inspected and any cracks found characterized using volumetric methods for crack depth. However, volumetric methods are not currently field-ready. The uncertainty in crack growth rates precludes justifiable predictions of the time required for a crack to progress from 10% to 75% through wall. Inspection frequencies and sample sizes are based on the evaluation against criteria IWB-3514.1 and IWB-3640, ranging from the inspection of one canister per site every 5 years for sites with canisters with no signs of corrosion to the inspection of all canisters with similar time in service (± 5 years) within 1 year after detection at sites where a crack exceeding the IWB-3640 limit is detected. While this guidance seems reasonable, it currently cannot be implemented and the technical underpinning has large uncertainty.

6. SUMMARY AND CONCLUSIONS

- Some of the most important processes and conditions thought to be involved in SCC at ISFSIs have been described. Many of these factors are interdependent, so full parameterization for an empirical model would require a large data set. Currently data are sparse and conflicting. Much was collected under conditions where at least one environmental condition (e.g., salt load) or material property (e.g., degree of sensitization) is set at a value that is at or beyond an extreme bound. Consequently data vary over several orders of magnitude.
- Considering this data, simplifying assumptions and professional judgment have been used in current empirical models. Three empirical models for SCC at ISFSIs have been described and their limitations discussed. The predictions of SCC growth rates penetration times vary greatly.
- It is the opinion of the authors of this report that currently the data and modeling do not provide a defensible technical basis for predicting a low probability of SCC penetration in 40 years. Thus, they have limited use in determining inspection frequency, and an operations-based and learning inspection frequency is necessary at this time.
- If it can be verified that the CGR slows down by two orders of magnitude at a depth between 1 and 3 mm, or if a technically sound chloride density threshold model for relevant conditions can be established, prediction of low probability of SCC penetration in 40 years may be possible, especially for inland sites. Such predictions would provide the technical basis for site-specific inspection frequencies. The inspection required at license renewal can determine a chloride density distribution, which will provide input to and validation of the prediction of SCC at that particular site, and thus help determine the timing of a second inspection.
- A summary and evaluation of the sections of the Calvert Cliffs Dry Cask Storage AMP and NUREG-1927 R1 draft for comment (NRC 2015) relevant to SCC sample frequency are provided.
- It is recommended that a comparison of the risk to the public from undetected through wall cracks and the dose to workers during inspections be performed to inform the frequency and sample size of inspections.
- In the meantime (while additional data is collected and refined predictive models are developed), an operations-based and learning inspection frequency as indicated in Section 3.6.1.10 under "Learning AMPs" of NUREG-1927 R1 Draft for Comment (NRC 2015) and recommended by the NEI through their tollgates and learning AMPs (NEI 2014) is appropriate. Sample tollgates from Appendix A of NEI 13-03 (NEI 2014) are provided in Appendix B.

7. REFERENCES

10 CFR Part 72. *Licensing Requirements for the Independent Storage of Spent Nuclear Fuel and High-Level Radioactive Waste.* U.S. Nuclear Regulatory Commission, Washington, D.C.

Albores-Silva O, E Charles, and C Padovani. 2011. *Effect of Chloride Deposition on Stress Corrosion Cracking of 316L Stainless Steel Used for Intermediate Level Radioactive Waste Containers*. Corrosion Engineering, Science and Technology. Vol. 46. No. 2. pp. 124-128.

Broussard J and S Chu. 2015. *Susceptibility Assessment Criteria for Chloride-Induced Stress Corrosion Cracking (CISCC) of Welded Stainless Steel Canisters for Dry Cask Storage Systems*. Presentation at the 04/21/2015 NRC Public Meeting with the Nuclear Energy Institute on the Chloride Induced Stress Corrosion Cracking Regulatory Issue Resolution Protocol. ML15146A11. U.S. Nuclear Regulatory Commission, Washington, D.C.

Bryan C, C Sallaberry1, R Dingreville1, C Stockman, H Adkins, and M Sutton. 2015. *Probabilistic Performance Assessment: SCC of SNF Interim Storage Canisters.* In Proceedings of the 15th International High-Level Radioactive Waste Management Conference (IHLRWMC). April 12-16, 2015. Charleston, SC. American Nuclear Society, La Grange Park, Illinois.

Bryan C and D Enos. 2015a. *SNF Interim Storage Canister Corrosion and Surface Environment Investigations.* FCRD-UFD-2015-000511. Sandia National Labs, Albuquerque, NM.

Bryan CR and DG Enos. 2015b. *Analysis of Dust Samples Collected from an Unused Spent Nuclear Fuel Interim Storage Container at Hope Creek, Delaware*, SAND2015-1746. Albuquerque, NM. Sandia National Laboratories.

Bryan CR and DG Enos. 2014. *Analysis of Dust Samples Collected from Spent Nuclear Fuel Interim Storage Containers at Hope Creek, Delaware, and Diablo Canyon, California*. SAND2014-16383. Sandia National Laboratories, Albuquerque, New Mexico.

Caseres L and TS Mintz. 2010. *Atmospheric Stress Corrosion Cracking Susceptibility of Welded and Unwelded 304, 304L, and 316L Austenitic Stainless Steels Commonly Used for Dry Cask Storage Containers Exposed to Marine Environments*. NUREG/CR-7030, U.S. Nuclear Regulatory Commission, Washington, D.C.

Chen Z and R Kelly. 2010. *Computational Modeling of Bounding Conditions for Pit Size on Stainless Steel in Atmospheric Environments.* Journal of the Electrochemical Society, 157(2), C69-C78.

Cook A, N Stevens, J Duff, A Mishelia, TS Leung, S Lyon, J Marrow, W Ganther, and I Cole. 2011. *Atmospheric-Induced Stress Corrosion Cracking of Austenitic Stainless Steels under Limited Chloride Supply.* Proc. 18th Int. Corros. Cong., Perth, Australia

Dai Q, J Hu, and M Salmeron. 1997. *Adsorption of Water on NaCl (100) Surfaces: Role of Atomic Steps.* The Journal of Physical Chemistry B 101, 1994-1998.

Dingreville R, C Sallaberry, C Bryan, C Stockman, H Adkins, and M Sutton, 2014. *Uncertainty Quantification Methodologies Development for Storage and Transportation of Used Nuclear Fuel: Pilot Study on Stress Corrosion Cracking of Canister Welds.* SAND2014-19467, OUO, Sandia National Laboratories.

Engelhardt G, and DD Macdonald. 1998. *Deterministic Prediction of Pit Depth Distribution*. Corrosion 54(6): 469–479, 1998.

Electric Power Research Institute (EPRI). 2015. *Susceptibility Assessment Criteria for Chloride-Induced Stress Corrosion Cracking (CISCC) of Welded Stainless Steel Canisters for Dry Cask Storage Systems*. TR 3002005371. EPRI. Palo Alto, CA.

EPRI. 2014a. *Used Fuel Dry Storage Stainless Steel Canister Stress Corrosion Cracking Susceptibility Assessment: R&D Roadmap Leading to Identification of Canisters Potentially Susceptible to Stress-Corrosion Cracking. Rev.1*. Electric Power Research Institute, Palo Alto, California.

EPRI. 2014b. *Literature Review of Environmental Conditions and Chloride-Induced Degradation Relevant to Stainless Steel Canisters in Dry Cask Storage Systems.* Report Number 3002002528. Electric Power Research Institute, Palo Alto, CA.

EPRI. 2014c. *Flaw Growth and Flaw Tolerance Assessment for Dry Cask Storage Canisters*. Report Number 3002002785, Electric Power Research Institute, Palo Alto, CA.

EPRI. 2014d. *Calvert Cliffs Stainless Steel Dry Storage Canister Inspection.* EPRI, Palo Alto, CA.

EPRI. 2013a. *Used Fuel Dry Storage Stainless Steel Canister Stress Corrosion Cracking Susceptibility Assessment: R&D Roadmap Leading to Identification of Canisters Potentially Susceptible to Stress-Corrosion Cracking. Rev.0.* ML13042A140. U.S. Nuclear Regulatory Commission, Washington, D.C.

EPRI. 2013b. *Failure Modes and Effects Analysis (FMEA) of Welded Stainless Steel Canisters for Dry Cask Storage Systems*. Report Number 3002000815. Electric Power Research Institute, Palo Alto, California.

Fairweather N, N Platts, and D Tice. 2008. *Stress-Corrosion Crack Initiation of Type 304 Stainless Steel in Atmospheric Environments Containing Chloride: Influence of Surface Condition Relative Humidity Temperature and Thermal Sensitization*. CORROSION 2008.

Greenspan L. 1977. *Humidity Fixed Points of Binary Saturated Aqueous Solutions.* Journal of Research of the National Bureau of Standards, Vol. 81A, No. 1.

Hayashibara H, M Mayuzumi, Y Mizutani, and J Tani. 2008. *Effects of Temperature and Humidity on Atmospheric Stress Corrosion Cracking of 304 Stainless Steel.* Paper No. 08492. Corrosion 2008 Conference & Expo. NACE International, Houston Texas.

He X, T Mintz, R Pabalan, L Miller, and G Oberson. 2014a. *Assessment of Stress Corrosion Cracking Susceptibility for Austenitic Stainless Steels Exposed to Atmospheric Chloride and Non-Chloride Salts.* NUREG-7170, ML14051A417. U.S. Nuclear Regulatory Commission, Washington, D.C.

He X, R Benke, Y-M Pan, L Caseres, P Shukla, K Chiang, R Pabalan, G Willden, and D Vickers. 2014b. *Available Methods for Functional Monitoring of Dry Cask Storage Systems*. ML14323A067, U.S. Nuclear Regulatory Commission, Washington, D.C.

Jones RH. 2003. *Stress-Corrosion Cracking, Corrosion: Fundamentals, Testing, and Protection, Vol 13A*, ASM Handbook, ASM International, 2003, p 346–366.

Kelly RG, A Aganval, F Cui, X Shan, U Landau and JH Payer. 2006. *Considerations of the Role of the Cathodic Region in Localized Corrosion*. MOL.20060705.0167. Yucca Mountain Project, U.S. Department of Energy. (Available at https://www.osti.gov/servlets/purl/893928-5RrmfH/)

Khatak H, J Gnanamoorthy, and P Rodriguez. 1996. *Studies on the Influence of Metallurgical Variables on the Stress Corrosion Behavior of AISI 304 Stainless Steel in Sodium Chloride Solution Using the Fracture Mechanics Approach*. Metallurgical and Materials Transactions A 27, 1313-1325.

Kondo Y. 1989. *Prediction of Fatigue Crack Initiation Life Based on Pit Growth*. Corrosion, 45(1), 7-11.

Kosaki A. 2008. *Evaluation Method of Corrosion Lifetime of Conventional Stainless Steel Canister under Oceanic Air Environment.* Nuclear Engineering and Design 238(5):1233–1240.

Krouse D, N Laycock, and C Padovani. 2014. *Modelling Pitting Corrosion of Stainless Steel in Atmospheric Exposures to Chloride Containing Environments*. Corrosion Engineering, Science and Technology, 49(6), 521-528.

Kuniya J, I Masaoka and R Sasaki. 1988. *Effect of Cold Work on the Stress Corrosion Cracking of Nonsensitized AISI 304 Stainless Steel in High-Temperature Oxygenated Water.* Corrosion 44(1), 21-28.

Kusnick J, M Benson, and S Lyons. 2013. *Finite Element Analysis of Weld Residual Stresses in Austenitic Stainless Steel Dry Cask Storage System Canisters*. ML13330A512. U.S. Nuclear Regulatory Commission, Washington, D.C.

Malm WC, BA Schichtel, ML Pitchford, IL Ashbaugh and RA Eldred. 2003. *Spatial and Month Trends in Speciated Fine Particle Concentration in the United States*. Journal of Geophysical Research 109, pp. 1-22.

Massari J and M Massoud. 2011. *2011 Update of ISFSI USAR DSC Leakage Dose Analyses*. Calculation CA07718, ML11364A025, Calvert Cliffs Nuclear Power Plant, LLC.

Mayuzumi M, J Tani, and T Arai. 2008. *Chloride Induced Stress Corrosion Cracking of Candidate Canister Materials for Dry Storage of Spent Fuel.* Nuclear Engineering and Design, 238(5), 1227-1232.

Meyer RM, AF Pardini, J Cuta, H Adkins, A Casella, A Qiao, M Larche, A Diaz, and S Doctor. 2013. *NDE to Manage Atmospheric SCC in Canisters for Dry Storage of Spent Fuel: An Assessment.* PNNL-22495, ML13276A196, Pacific Northwest National Laboratory, Richland, WA.

Nakayama G and Y Sakakibara. 2013. *Prediction Model for Atmospheric Stress Corrosion Cracking of Stainless Steel*. ECS Transactions, 50 (31) 303-311.

Nakayama G. 2006. *Atmospheric Stress Corrosion Cracking (ASCC) Susceptibility of Stainless Alloys for Metallic Containers.* In: VanIseghem, P. (ed.) Scientific Basis for Nuclear Waste Management XXIX, pp. 845-852.

NEI. 2014. *Guidance for Operations-Based Aging Management for Dry Cask Storage.* NEI 14-03 Revision 0. ML14266A225, Nuclear Energy Institute, Washington D.C.

Nishikata A, Y Ichihara, Y Hayashi and T Tsuru. 1997. *Influence of Electrolyte Layer Thickness and pH on the Initial Stage of the Atmospheric Corrosion of Iron*. J. Electrochem. Soc. 1997. Volume 144, Issue 4, pp 1244-1252.

Nuclear Decommissioning Authority (NDA). *Industry Guidance - Interim Storage of Higher Activity Waste Packages – Integrated Approach.* NDA. West Cumbria, UK (2012).

NEI. 2014. *Guidance for Operations-Based Aging Management for Dry Cask Storage.* NEI 14-03. ML14266A225. U.S. Nuclear Regulatory Commission, Washington, D.C.

Newman JC and IS Raju. 1981. *An Empirical Stress-Intensity Factor Equation for the Surface Crack.* Engineering Fracture Mechanics Vol. 15, No. 1-2, pp. 185-192.

Newman JC and IS Raju. 1979. *Analyses of Surface Cracks in Finite Plates under Tension or Bending Loads.* NASA Technical Paper 1578.

NRC. 2015. *Standard Review Plan for Renewal of Specific Licenses and Certificates of Compliance for Dry Storage of Spent Nuclear Fuel.* NUREG-1927 R1 Draft Report for Comment. ML15180A011. U.S. Nuclear Regulatory Commission, Washington, D.C.

NRC. 2014a. *Attachment 2 Used Fuel Storage and Transportation Issue Resolution Plan Issue Number: N-10-01, Title: Dry Spent Fuel Storage Canister Chloride Induced Stress Corrosion Cracking*, ML14309A572. U.S. Nuclear Regulatory Commission, Washington, D.C.

NRC. 2014b. *Identification and Prioritization of the Technical Information Needs Affecting Potential Regulation of Extended Storage and Transportation of Spent Nuclear Fuel.* ML14043A423. U.S. Nuclear Regulatory Commission, Washington, D.C.

NRC. 2014c. *Safety Evaluation Report for License Renewal, Calvert Cliffs Nuclear Power Plant, Independent Spent Fuel Storage Installation, Docket No. 72-08, License No. SNM-2505,* ML14274A038. U.S. Nuclear Regulatory Commission, Washington, D.C.

NRC. 2014d. *Enclosure: Safety Evaluation Report, Appendix A, Revised Aging Management Programs, SNM-2505, 72-8 [Letter To G. H. Gellrich re: Issuance of Renewed Materials License No. SNM-2505 for the Calvert Cliffs Site Independent Spent Fuel Storage Installation]*. ML14274A041. U.S. Nuclear Regulatory Commission, Washington, D.C.

NRC. 2012. *Information Notice 2012-20: Potential Chloride-Induced Stress Corrosion Cracking of Austenitic Stainless Steel and Maintenance of Dry Cask Storage System Canisters*. U.S. Nuclear Regulatory Commission, Washington, D.C.

NRC. 2011. *Standard Review Plan for Renewal of Spent Fuel Dry Cask Storage System Licenses and Certificates of Compliance*. NUREG-1927, U.S. Nuclear Regulatory Commission, Washington, D.C.

Oak Ridge National Laboratory (ORNL). 2015. *Rationale for the Performance Specification for Standardized Transportation, Aging, and Disposal Canister Systems.* FCRD-NFST-2015-000106, Rev. 1 ORNL/SPR-2015/252. Prepared for the US Department of Energy Used Fuel Disposition Campaign, Washington, DC. http://curie.ornl.gov/content/performance-specification-and-rationale-standardized-transportation-aging-and-disposal

Parish OO and TW Putnam. 1977. *Equations for the Determination of Humidity from Dewpoint and Psychrometric Data*. NASA Technical Note, TN D-8401.

Parrott R and H Pitts. 2011. *Chloride Stress Corrosion Cracking in Austenitic Stainless Steel: Assessing Susceptibility and Structural Integrity*. RR902, U.K. Health and Safety Executive. Buxton, Derbyshire, UK.

Peguet L, B Malki, and B Baroux. 2007. *Influence of Cold Working on the Pitting Corrosion Resistance of Stainless Steels*. Corrosion Science 49 (2007), 1933-1948.

Pio CA and DA Lopes. 1998. *Chlorine Loss from Marine Aerosol in a Coastal Atmosphere*. Journal of Geophysical Research-Atmospheres 103, 25263-25272.

Prosek T, A LeGac, D Thierry, S Le Manchet, C Lojewski, A Fanica, E Johansson, C Canderyd, F Dupoiron, T Snauwaert, F Maas, and B Droesbeke. 2014. *Low-Temperature Stress Corrosion Cracking of Austenitic and Duplex Stainless Steels Under Chloride Deposits*, Corrosion, Vol. 70, No. 10, pp. 1052-1063.

Prosek T, A Iversen, and C Taxén. 2009. *Low Temperature Stress Corrosion Cracking of Stainless Steels in the Atmosphere in Presence of Chloride Deposits*. Corrosion 65, 105-117.

Renshaw J. 2014. *NDE for Dry Canister Storage System Inspection.* Presentation at the EPRI ESCP Meeting December 3, 2014 in Charlotte, NC.

Schindelholz E, LK Tsui, RG Kelly. 2014a. *Hygroscopic Particle Behavior Studied by Interdigitated Array Microelectrode Impedance Sensors,* J Phys Chem A, Vol. 118, No. 1, pp. 167-177, http://www.ncbi.nlm.nih.gov/pubmed/24328164.

Schindelholz E, B Risteen, and R Kelly. 2014b. *Effect of Relative Humidity on Corrosion of Steel under Sea-salt Aerosol Proxies I. NaCl*. Journal of the Electrochemical Society 161(10), C450-C459.

Schindelholz E, B Risteen, and R Kelly. 2014c. *Effect of Relative Humidity on Corrosion of Steel under Sea-salt Aerosol Proxies II. $MgCl_2$, Artificial Seawater*. Journal of the Electrochemical Society 161(10), C460-C470.

Schindelholz E and RG Kelly. 2012. *Wetting Phenomena and Time of Wetness in Atmospheric Corrosion: A Review*. Corrosion Reviews. Vol. 30, No. 5-6, pp. 135-170.

Scheiner S and C Hellmich. 2007. *Stable Pitting Corrosion of Stainless Steel as Diffusion-Controlled Dissolution Process with a Sharp Moving Electrode Boundary*. Corrosion Science, Vol. 49, No. 2, pp. 319-346.

Shirai K, J Tani, M Gotoh, M Wataru. 2012. *SCC Evaluation Method of Multi-Purpose Canister in Long Term Storage*. Proceedings of PSAM 11 & ESREL, (16BS-We2-3).

Shirai K, J Tani, T Arai, M Wataru, H Takeda, and T Saegusa. 2011a. *SCC Evaluation Test of a Multi-Purpose Canister*. In Proceedings of the 13th International High-Level Radioactive Waste Management Conference (IHLRWMC) April 10-14, 2011, Albuquerque, New Mexico, pp. 824-831. American Nuclear Society, La Grange Park, Illinois.

Shirai K, J Tani, and T Saegusa. 2011b. *Study on Interim Storage of Spent Nuclear Fuel by Concrete Cask for Practical Use - Feasibility Study on Prevention of Chloride Induced Stress Corrosion Cracking for Type 304L Stainless Steel Canister*. CRIEPI N10035. (In Japanese)

Shoji S and N Ohnaka, 1989. *Effects of Relative Humidity and Chloride Type on Stainless Steel Room-Temperature Atmospheric Corrosion Cracking*. Corrosion Engineering, Vol. 38, p. 111-119, 1989.

SNL. 2007. *In-Drift Precipitates/Salts Model*, ANL-EBS-MD-000045 REV 03. Las Vegas, NV. Sandia National Laboratories.

Spiedel MO. 1977. *Stress Corrosion Crack Growth in Austenitic Stainless Steel*. Corrosion. Vol. 33, No. 6, pp. 199-202.

Stockman C, BD Hanson, SC Marschman, HA Alsaed, KB Sorenson. 2014. *Used Nuclear Fuel Extended Storage and Transportation Research and Development Review and Plan.* FCRD-UFD-2014-000050. SAND2014-19594 R. Prepared for the US Department of Energy Used Fuel Disposition Campaign, Washington, DC.

Suffield S, JA Fort, JM Cuta, HE Adkins, BA Collins, and ER Siciliano. 2012. *Thermal Modeling of NUHOMS HSM15 and HSM-1 Storage Modules at Calvert Cliffs Nuclear Power Station ISFSI*. FCRD-UFD-2012-000344. PNNL-21788. Prepared for the US Department of Energy Used Fuel Disposition Campaign, Washington, DC. .http://www.osti.gov/scitech/biblio/1055414

Tani J, M Mayuzumi, and N Hara. 2009. *Initiation and Propagation of Stress Corrosion Cracking of Stainless Steel Canister for Concrete Cask Storage of Spent Nuclear Fuel.* Corrosion 65(3):187-194.

Taylor MF. 1994. *The Significance of Salt Contamination on Steel Surfaces, Its Measurement and Removal.* UK Corrosion and Eurocorr 94:31 October-3 November 1994, Bournemouth International Centre, UK.

Tokiwai M, H Kimura, and H Kusanagi. 1985. *The Amount of Chlorine Contamination for Prevention of Stress Corrosion Cracking in Sensitized Type 304 Stainless Steel.* Corrosion Science, 25(8), 837-844.

Tomashov ND. 1964. *Development of the Electrochemical Theory of Metallic Corrosion*. Corrosion 20(1), 7t-14t.

Turnbull A. 2014. *Corrosion Pitting and Environmentally Assisted Small Crack Growth.* Proceedings of the Royal Society A: Mathematical, Physical and Engineering Science 470, 20140254.

Turnbull A, D Horner, and B Connolly. 2009. *Challenges in Modelling the Evolution of Stress Corrosion Cracks from Pits.* Engineering Fracture Mechanics. Vol. 76, No. 5, pp. 633-640.

Turnbull A, L McCartney, and S Zhou. 2006a. *Modelling of the Evolution of Stress Corrosion Cracks from Corrosion Pits*. Scripta Materialia 54, 575-578.

Turnbull A, L McCartney, and S Zhou. 2006b. *A Model To Predict the Evolution of Pitting Corrosion and the Pit-To-Crack Transition Incorporating Statistically Distributed Input Parameters*. Corrosion Science 48, 2084-2105.

Turnbull A and S Zhou. 2004. *Pit to Crack Transition in Stress Corrosion Cracking of a Steam Turbine Disc Steel.* Corrosion Science 46, 1239-1264.

Wall SM, W John, and JL Ondo. 1988. *Measurement of Aerosol Size Distributions for Nitrate and Major Ionic Species.* Atmospheric Environment (1967) Vol. 22, Issue 8, pp. 1649-1656.

Woldemedhin MT and RG Kelly. 2014. *Evaluation of the Maximum Pit Size Model on Stainless Steel under Atmospheric Conditions,* ECS Transactions, 58(29), 41-50.

Wolery TW and RL Jarek. 2003. *Software User's Manual, EQ3/6 Version 8.0.* Albuquerque, NM. Sandia National Laboratories.

Wu G, and M Modarres. 2012. *A Probabilistic-Mechanistic Approach to Modeling Stress Corrosion Cracking in Alloy 600 Components with Applications*. PSAM 2011.

Zhang X-Y, S-X Li, and R Liang. 2013. *Effect of Corrosion Pits on Fatigue Life and Crack Initiation*. Proceedings ICF13.

APPENDIX A:
Pertinent Sections of NUREG-1927 R1 Draft for Comment

Appendix A: Pertinent Sections of NUREG-1927 R1 Draft for Comment

…1.4.7 Conditions to Specific Licenses and CoCs in the Period of Extended Operation

…The NRC staff is also likely to renew a license or CoC with a condition requiring the applicant to update, revise, or create procedures for implementing the activities in the AMPs. These procedures will be subject to inspection to ensure they are maintained, implemented, and periodically updated to respond to operating experience and valid consensus codes and standards, while providing reasonable assurance that the pertinent SSCs maintain their intended function.

As the entirety of the AMP may not be included in the CoC or technical specifications, site procedures for AMP implementation may later be changed. Therefore, additional conditions or technical specifications may be required in the specific license or CoC to ensure critical elements of the AMPs are effectively maintained. These conditions should be specific to information in the AMP described in the renewal application which staff relied upon to make the requisite safety findings of reasonable assurance of adequate protection of public health and safety, and the environment…

…3.4.1.3 Aging Management Activities

The reviewer should ensure that the applicant has identified those aging mechanisms and effects requiring either an AMP or TLAA. Figure 3-1 illustrates the process for handling those SSCs that are determined to be within the scope of renewal and subject to a potential aging effect. The AMR defines two methods for addressing potential aging mechanisms and effects: TLAA (Section 3.5) and AMP (Section 3.6).

The NRC may condition the approval of a renewal on the requirements of a given AMP being met during the period of extended operation (see Section 1.4.7). The CoC user (general licensee) would ordinarily carry out the activities described in this AMP. Pursuant to 10 CFR 72.212(b)(11) and 10 CFR 72.240(e), the NRC may make the AMP applicable to the general licensee by adding the appropriate condition(s) or technical specification(s) to the renewed CoC. Specific licenses may also be similarly conditioned (see Section 1.4.7)….

…3.6 Aging Management Programs

Aging management programs (AMPs) monitor and control the degradation of SSCs within the scope of renewal so that aging effects will not result in a loss of intended functions during the period of extended operation. An AMP includes all activities that are credited for managing aging mechanisms or effects for specific SSCs, including activities conducted during the initial storage period. An effective AMP prevents, mitigates, or detects the aging effects and provides or the prediction of the extent of the effects of aging and timely corrective actions before there is a loss of intended function.

Aging management programs should be informed, and enhanced when necessary, based on the ongoing review of both site-specific and industry-wide operating experience, including relevant international and non-nuclear operating experience. Operating experience provides direct confirmation of the effectiveness of an AMP and critical feedback for the need for improvement. As new knowledge and data become available from new analyses, experiments, and operating experience, licensees and CoC holders should revise existing AMPs (or pertinent procedures for AMP implementation) to address program improvements or aging issues.

…3.6.1 Review Guidance

An AMP should contain the following 10 elements:

1. Scope of Program,

2. Preventive actions,

3. Parameters monitored or inspected,

4. Detection of aging effects,

5. Monitoring and trending,

6. Acceptance criteria,

7. Corrective actions,

8. Confirmation process,

9. Administrative controls, and

10. Operating experience…

…3.6.1.4 Detection of Aging Effects

Detection of aging effects should occur before there is a loss of intended function for any SSC identified within the scope of the program. This element should include inspection and monitoring details, including method or technique (i.e., visual, volumetric, surface inspection), frequency, sample size, data collection, and timing of inspections to ensure timely detection of aging effects. In general, the information in this element describes the "when," "where," and "how" of the AMP (i.e., the specific aspects of the activities to collect data as part of the inspection or monitoring activities).

The reviewer should ensure that the applicant has provided sufficient details on the following aspects of the inspection or monitoring activities:

- Method or technique: The method should be adequate and proven to be capable of evaluating the condition of the SSC against the acceptance criteria for the specific aging mechanism or effect being monitored or inspected (as defined in AMP Element 6). For example, the applicant should provide a valid technical basis that a particular instrument has sufficient resolution to identify a specific crack or defect dimension.

- Frequency: The reviewer should ensure that the proposed intervals for inspection or monitoring are consistent with applicable site-specific or industry-wide operating experience. Inspections should have sufficient frequency to ensure that intended functions will be maintained until the next scheduled inspection.

- Sample size: The application should identify and justify the number of SSCs to be evaluated per inspection, including the extent of the inspection for each SSC (e.g., all accessible areas of five concrete overpacks in service). The reviewer should ensure the applicant has justified the use of a limited sample size (e.g., one cask per pad) with a technical basis, which should include applicable site-specific and industry-wide operating experience. The application should also define the areas that have been determined to be inaccessible or below-grade and propose how the condition of the inaccessible SSCs will be assessed. The reviewer should ensure that the scope of each inspection is properly defined for both accessible and inaccessible (including below-grade) areas.

- Data collection: The application should reference any specific methods to be used for data acquisition, including any applicable consensus codes and standards. For example, the application

may reference field evaluation guides for evaluating and documenting cracks in concrete (e.g., ACI 224.1R, ACI 201.1R).

- Timing of inspections: The application may include results of a lead system inspection to serve as a baseline for the implementation of the AMP, which should be performed in accordance to Appendix C of this guidance. The reviewer should also consider any specific information on the proposed inspection schedule (e.g., time of the year) to support the effective detection of aging effects before a loss of intended function.

…3.6.1.5 Monitoring and Trending

Monitoring and trending should provide for an evaluation of the extent of the effects of aging and the need for timely corrective or mitigative actions. This element describes how the data collected will be evaluated. This includes an evaluation of the results against the acceptance criteria and an evaluation regarding the rate of degradation in order to ensure that the timing of the next scheduled inspection will occur before a loss of intended function….

…3.6.1.6 Acceptance Criteria

The acceptance criteria, against which the need for corrective action will be evaluated, should ensure that the SSC intended functions and the approved design bases are maintained during the period of extended operation. The proposed acceptance criteria should be appropriately justified.

The acceptance criteria could be specific numerical values or could consist of a discussion of the process for calculating specific numerical values of conditional acceptance criteria to ensure that the design bases are maintained. The reviewer should ensure that the acceptance criteria:

- Include a quantitative basis (justifiable by operating experience, engineering analysis, consensus codes/standards),
- Avoid use of non-quantifiable phrases (e.g., significant, moderate, minor, little, slight, few), and
- Are achievable and actionable, that is, the method/technique is qualified to meet the stated quantitative criteria (e.g., sufficient resolution/sensitivity).

The acceptance criteria may be taken directly from the design bases information included in either the final safety analysis report (FSAR) or technical specifications. The acceptance criteria also may be established by methodologies provided in NRC-approved topical reports or appropriate codes and standards.

… 3.6.1.10 Operating Experience

…Learning AMPs

The reviewer should ensure that applicants commit to future reviews of site-specific and industry-wide operating experience, including relevant international and non-nuclear operating experience, to confirm the effectiveness of their AMPs or indicate a need to enhance or modify an AMP. The commitment to future reviews should ensure that, as knowledge and data become available from new analyses, experiments, and operating experience, the licensees and CoC holders will revise the existing AMPs (or pertinent procedures for AMP implementation) as necessary to address any deficiencies identified during the review of operating experience (see Figure 3-2).

If an applicant follows this approach, the reviewer should ensure that the description of the periodic assessments includes specific performance criteria (e.g., program-specific performance indicators for each

of the 10 AMP elements) and proposed actions based on the assessment findings. The reviewer should also ensure that the timing of the assessments appropriately considers the rate of aging degradation and the anticipated availability of data from industry initiatives. The reviewer should consider the frequency, acceptance criteria, and proposed corrective actions for these assessments for the requisite finding of reasonable assurance.

Nuclear Energy Institute (NEI) 14-03, "Guidance for Operations-Based Aging Management for Dry Cask Storage," Rev. 0, provides a proposed framework for learning AMPs through the use of "tollgates." NEI 14-03 defines "tollgates" as periodic points within the period of extended operation when licensees would be required to document an aggregate safety assessment. Tollgates are described as an additional set of in-service assessments beyond the normal continual assessment of operating experience, research, monitoring, and inspections on DSS component performance that is part of normal ISFSI operations for licensees during the initial storage period as well as the period of extended operation. NEI 14-03 states that licensees will be obligated to comply with any tollgate license or CoC conditions approved as part of the license or CoC renewal. The reviewer should be aware that an applicant may reference the use of "tollgates" in the renewal application. The reviewer should (1) assess the applicant's proposed periodic assessments of operating experience and other relevant data, and (2) make a determination regarding the ability of these assessments to ensure the continued effectiveness of AMPs. The reviewer should ensure that tollgates determined necessary to demonstrate the continued effectiveness of the AMPs are included as a condition of the renewed license or CoC.

NEI 14-03, Rev. 0, also describes a general framework for the aggregation and dissemination of operating experience across the industry through the use of an operating experience "clearinghouse." Whether the applicant references the clearinghouse described in NEI 14-03 or proposes an alternative means to seek out operating experience, the reviewer should ensure that the application describes how industry-wide operating experience and results of industry initiatives will be accessed and utilized to ensure that AMPs are modified as appropriate…

…Appendix B

…Example AMP for Localized Corrosion and Stress Corrosion Cracking of Welded Stainless Steel Dry Storage Canisters

…Element 4 Detection of Aging Effects

…Visual Examination
…Procedures for remote visual examination should be performance demonstrated; procedure attributes including equipment resolution, lighting requirements, etc., should reference applicable standards, such as ASME Section XI, Article IWA-2200 for VT-1 and VT-3 examinations (ASME, 2007) and BWRVIP-03 (Selby 2005) for EVT-1 examinations.

Volumetric Examination
Additional assessment is necessary for suspected areas of localized corrosion and/or stress corrosion cracking. In these cases, the severity of degradation must be assessed including the dimensions of the affected area and the depth of penetration with respect to the thickness of the canister. For accessible areas where adequate cleaning can be performed, remote visual inspection meeting the requirements for VT-1 Examination (ASME Section XI, IWA-2211) may be used to determine the type of degradation present (e.g., pitting corrosion or stress corrosion cracking) and the location of degradation. Examinations to characterize the extent and severity of localized corrosion and/or stress corrosion

cracking should be conducted using surface and/or volumetric inspection techniques consistent with the requirements of ASME Section XI, IWB-2500 for category B-J components (ASME, 2007)

Sample Size
Minimum of one canister at each site. …

Frequency
Once every 5 years…

…Element 6 Acceptance Criteria

No indications of localized corrosion pits, etching, crevice corrosion, stress corrosion cracking, red-orange colored corrosion products emanating from crevice locations, or red-orange colored corrosion products in the vicinity of canister fabrication welds, closure welds, and welds associated with temporary attachments during canister fabrication.

Confirmed or suspected areas of crevice corrosion, pitting corrosion and stress corrosion cracking must be assessed in accordance with acceptance standards identified in ASME Section XI, IWB-3514. Flaws exceeding the acceptance standards in IWB-3514.1 must be evaluated using the acceptance criteria identified in IWB-3640.

Indications Requiring Additional Evaluation

Although shop and handling procedures include controls to prevent iron contamination of the stainless steel surfaces, contamination does occur and is usually identified by rust-colored surface deposits. Iron contamination can exacerbate CISCC in stainless steels. In accessible locations, removal of the deposits and rust stains that reveal undamaged welds (i.e., absence of pits, crack, localized attack, or etching) and the original machining/grinding marks on the stainless steel base metal, including weld heat affected zones, may be used to confirm that localized corrosion or stress corrosion cracking have not been initiated.

Indications of interest that are subject to additional examination and disposition include:

[They list the same as above, but are more specific. Corrosion patches that are greater ≥1 mm in diameter, corrosion products at crevices, liner indications, or tubercles of any size must be further evaluated.]

…Element 7 Corrective Actions

…Extent of Condition

Confirmation of localized corrosion and/or stress corrosion cracking requires inspection of additional canisters at the same location to determine the extent of condition. Priority for additional inspections should be to canisters with similar time in service and initial loading.

Disposition of Canisters with Aging Effects

For austenitic stainless steel canisters covered by an AMP that utilizes the inspection and acceptance criteria in ASME B&PV code Section XI for Class 1 piping system, the disposition of canisters should be commensurate with in-service inspection results:

- Canisters with no evidence of corrosion are permitted to remain in service and will continue to be inspected at 5-year intervals.

- Canisters with rust deposits that are determined to be a result of iron contamination but do not have evidence of localized corrosion or stress corrosion cracking are permitted to remain in service and will continue to be inspected at 5-year intervals.
- Canisters that show evidence of localized corrosion and/or stress corrosion cracking that does not exceed the acceptance standards in IWB-3514.1 are permitted to remain in service and will be inspected at 5-year intervals. Sample size will be increased to assess 25 percent of canisters with similar time in service (± 5 years) or a minimum of one additional canister with a time in service closest to the original sample within one year of the completed in-service inspection date. Results of the initial inspection and the schedule for additional inspections will be reported to the NRC. In addition, the results for the additional in-service inspections will be reported to the NRC upon completion.
- Canisters that show evidence of localized corrosion and/or stress corrosion cracking that exceeds the acceptance standards in IWB-3514.1 but meet the acceptance criteria identified in IWB-3640 are permitted to remain in service and will be inspected at 3-year intervals. Sample size will be increased to assess 50 percent of canisters with similar time in service (± 5 years) or a minimum of one additional canister with a time in service closest to the original sample within one year of the completed in-service inspection date. Results of the initial inspection and the schedule for additional inspections will be reported to the NRC. In addition, the results for the additional in-service inspections will be reported to the NRC upon completion.
- Canisters that show evidence of localized corrosion and/or stress corrosion cracking that exceeds acceptance criteria identified in IWB-3640 are not permitted to remain in service. Upon identification, the in-service inspection sample size will be increased to assess 100 percent of canisters with similar time in service (± 5 years) or a minimum of one additional canister with a time in service closest to the original sample within one year of the completed in-service inspection date. Results of the initial inspection, the schedule for mitigation either by repair or replacement and the schedule for additional inspections will be reported to the NRC. In addition, the results for the additional in-service inspections will be reported to the NRC upon completion….

APPENDIX B:
NEI 14-03 Appendix A: SAMPLE TOLLGATES

Appendix B: NEI 14-03 Appendix A: SAMPLE TOLLGATES

TOLL GATE	YEAR*	ASSESSMENT
1	A**	Evaluate information from the following sources and perform a written assessment of the aggregate impact of the information, including but not limited to trends, corrective actions required, and the effectiveness of the AMPs with which they are associated: • results, if any, of research and development programs focused specifically on age related degradation mechanisms identified as potentially affecting the storage system and ISFSI site, such as: – DOE/EPRI High Burnup Dry Storage Cask Research and Development Project" (HDRP) – EPRI Chloride-Induced Stress Corrosion Cracking (CISCC) research • relevant results of other domestic and international research (including non-nuclear) • relevant domestic and international operating experience (including non-nuclear) • relevant results of domestic and international ISFSI and DCSS performance monitoring • relevant results of domestic and international ISFSI and DCSS inspections. NOTE: Feedback on any of the above should be assessed at the time the
2	B	Evaluate additional information gained from the sources listed in Tollgate 1 along with any new relevant sources and perform a written assessment of the aggregate impact of the information. This evaluation should be informed by the results of Tollgate 1. The age related degradation mechanisms evaluated at this Tollgate and the time at which it is conducted may be adjusted based on the results of the Tollgate 1 assessment.
3	C	Same as Tollgate 1 as informed by the results of Tollgates 1 and 2 4
4	D	Same as Tollgate 1 as informed by the results of Tollgates 1, 2, and 3

* Based on the year first cask at the ISFSI reaches initial term of service and aging management activities are required.
** Timing of initial tollgate (A), tollgate frequency (B, C, etc.), and total number of tollgates to be determined by specific licensee/CoC holder in the renewal application. (NEI 2014)